University of Texas at Arlington

MavMatrix

2023

INVESTIGATION ON THE IMPACTS OF LAND SUBSIDENCE AND URBANIZATION ON FLOOD INUNDATION IN TEXAS

Han Jiang

INVESTIGATION ON THE IMPACTS OF LAND SUBSIDENCE AND

URBANIZATION ON FLOOD INUNDATION IN TEXAS

By

HAN JIANG

DISSERTATION

Presented to the Faculty of the Graduate School of

The University of Texas at Arlington

in Partial Fulfillment of the Requirements

for the Degree of

DOCTOR OF PHILOSOPHY

THE UNIVERSITY OF TEXAS AT ARLINGTON

August 2023

DEDICATION

This dissertation is dedicated to my

extraordinary parents, whose love, support, and

encouragement have carried me through this

journey. Additionally, this work is lovingly

dedicated to my faithful cat, Bamboo. This

journey would not have been the same without

each of you by my side.

ACKNOWLEDGEMENTS

First and foremost, I would like to express my gratitude to my adviser, Dr. Nick Z. Fang, for his constant and valuable guidance, encouragement, and mentorship throughout the journey of this research. His wisdom has been an inspirational beacon in my Ph.D. journey. I could not have hoped for a better supervisor. Without his inspiring feedback and support, this journey would have been significantly more challenging.

I would also like to thank my committee members, Professor Hummel, Professor Yi Liu, Professor Mattingly and Professor Yu Zhang for their insightful comments and constructive suggestions which have immensely contributed to shaping this work.

I would also like to thank the wonderful Fang Research Group members who are encouraging and supportive during these years. Without them, my research journey won't be complete. Special thanks to the University library staff and administrative personnel, who have been an integral part of this process.

Lastly, my heartfelt appreciation goes to my family and friends for their constant encouragement, emotional and practical support throughout this journey. I am eternally grateful.

ABSTRACT

INVESTIGATION ON THE IMPACTS OF LAND SUBSIDENCE AND

URBANIZATION CHANGE ON HYDROLOGY AND HYDRAULICS IN TEXAS

Han Jiang, Ph.D.

The University of Texas at Arlington, 2023

Floods, being a prevalent and catastrophic natural hazard, have resulted in enormous losses to human lives and properties all over the world. Hence, there is a pressing need to enhance urban resilience and to improve emergency response capacities in order to mitigate the risks posed by flood hazards. Many models have been developed by engineers to simulate and examine the hydrologic and hydraulic responses to the changes within the physical environment. However, there are still knowledge gaps in advancing the understanding of the H&H behavior and hydrodynamics modeling performance. This doctoral study aims to help bridge such gaps via assessing the impacts of land subsidence and urbanization on flooding. The findings of this research can provide valuable insights into understanding the changes of flood inundation results regarding land subsidence and urbanization, which can assist engineers and stakeholders in further research, decision making and flood emergency responses.

Table of Contents

Chapter 1: Introduction

RESEARCH GOALS

The overarching goals of this Ph.D. work are *1) to examine the change in topology due to a historical 120-year land subsidence, 2) to establish a hydrodynamic model that accurately reproduces the flood inundation of 2017 Hurricane Harvey, and (3) to investigate the change in Harvey flood inundation due to the historical land subsidence and change of urbanization in Brays Bayou.* Significant efforts have been made to enhance the capabilities and functionality of hydraulic modeling. Recent computational advances in computational provide new opportunities to support decision-making and adaptation. My Ph.D. study primarily focuses on bridging the gap between science and engineering via investigating hydraulic models in achieving realism and efficiency to better facilitate water resource management. To this end, the whole dissertation aims to answer the following research questions.

1. How is the reliability of HEC-RAS 2D modeling as an integrated hydrodynamic-hydrologic model with 2D mesh only?

2. Will flooding always get worse with subsiding land?

3. What effect does land subsidence have on flood characteristics (e.g., flood depth/extent/volume/velocity) in the watershed with and without the change on LULC from 1900 to 2045?

DISSERTATION STRUCTURE

This dissertation consists of five chapters. Chapter 1 introduces the research goals, questions and structure of this dissertation. Subsequent chapters contain two manuscripts focusing on evaluation of the impact of land subsidence and urbanization on flooding using a HEC-RAS 2D model (Chapter 2, 3, 4 and 5), Chapter 6 presents conclusions and future research and appendix provides additional information about the model and results.

Chapter 2 introduces the literature review of the importance of studying land subsidence and urbanization impact and related previous research. Chapter 3 presents the study area and the data used in this study. Chapters 4 and 5 show the methods and results for investigation of impact from land subsidence in a highly urbanized watershed using HEC-RAS software. The research examines the retroactive alterations in regional topology caused by 145 years (1900 to 2045) of land subsidence and investigates the impact of land subsidence and urbanization on flood inundation using HEC-RAS model. Land cover/land use data from multiple sources are used. These changes are analyzed using a high-resolution, physics-based model that simulates groundwater depletion and the resulting compaction of the aquifer system. The findings suggest that the impact of land subsidence on flood depth is very insignificant, with the flood water deepening by six centimeters for every meter of subsided land at the most severely affected site. The temporal relationship between land subsidence and flood depth demonstrates a significant nonlinearity, wherein the influence of prior land subsidence hotspots may be modified by subsequent and ongoing land subsidence.

Chapters 2 to 5 are two manuscripts published or intended for publication in peer-reviewed journals. Their full references are as follows:

Jiang, H., Zhang, J., Liu, Y., Li, J., & Fang, Z. N. (2023). "Does flooding get worse with subsiding land? Investigating the impacts of land subsidence on flood inundation from Hurricane Harvey". Science of the Total Environment, 865, 161072. DOI: https://doi.org/10.1016/j.scitotenv.2022.161072

Jiang. H., Li, D., Fakhrabadi. P., Zhang, J., Liu, Y., Li, J., & Fang, Z. N. (2024). "Investigation on the impact of land subsidence and urbanization on flood inundation in Brays Bayou, Texas". (In Preparation).

ACKNOWLEDGMENT

Chapter 2: Literature Review

Flood is one of the most destructive natural disasters throughout the world (Kellens et al., 2013; Munawar et al., 2019; Ahmadlou et al., 2021; Shareef and Abdulrazzaq, 2021). Not only does it pose a great threat to human beings and their living environment, but it also causes severe damage to the economy Flood is one of the most destructive natural disasters throughout the world (Kellens et al., 2013; Munawar et al., 2019; Ahmadlou et al., 2021; Shareef and Abdulrazzaq, 2021). Not only does it pose a great threat to human beings and their living environment, but it also causes severe damage to the economy (Penning-Rowsell et al., 2005; Khan et al., 2010; Michel-Kerjan and Kunreuther, 2011; Patel et al., 2017; Farooq et al., 2019; Kim et al., 2020). Based on the international disaster database, flooding has resulted in a total loss of over $870 billion globally since 1900 (EM-DAT, 2020). In the United States (U.S.) alone, flooding has caused more than $68 billion in loss between 1970 and 2019 (FEMA, 2020). As one of the most devastating events, 2017 Hurricane Harvey produced the largest rainfall of any U.S. hurricane on record (Emanuel, 2017) with the maximum four-day rainfall exceeding 1000-year return period in most of Houston-Beaumont region (HDSC, 2017). During the severe flooding caused by Hurricane Harvey, numerous houses damaged are located even outside of the 500-year floodplain areas (Jonkman et al., 2018; Miller and Shirzaei, 2019). The unprecedent nature of the Harvey floods calls for a significant advancement in understanding of the processes of determining flood risk and severity.

Besides climate variability and changes, several studies have shown that anthropogenic and natural changes to the land surface (e.g., land subsidence) might exacerbate flooding issues (e.g., Rodolfo and Siringan, 2006; Hanson et al., 2011; Viero et al., 2019; Ouyang et al., 2020).

Especially for the flat-lying coastal areas, land subsidence would increase the potential for flooding caused by tides and storm surges (Holzer and Johnson, 1985). Dixon et al. (2006) found the failure of the levees during Hurricane Katrina could be caused by land subsidence in New Orleans. A study done by Wang et al. (2012) indicated land subsidence affects coastal seawalls and flood-control levees in Shanghai, leading to changes in floodplain boundaries. Moreover, Ouyang et al. (2020) analyzed the local land subsidence caused by 2011 Tohoku earthquake in Japan and found the inundation areas would be underestimated by around 10 % if only considering rainfalls without considering the effect of land subsidence. The cause of land subsidence has been studied in several researches all over the world and groundwater withdrawal is found to be one of the most important causes of land subsidence (Sun et al., 1999; Teatini et al., 2005; Marfai and King, 2007; Pacheco-Martinez et al., 2015; Wang et al., 2019; Golian et al., 2021). In the U.S., land subsidence happens in many urbanized areas with over 44,000 km2 across 45 states, and among all the affected areas, the Houston-Galveston area experienced land subsidence as early as 1900s (Stork and Sneed, 2002). The main causes of land subsidence in this area are the exploitation of groundwater, extraction of oil and gas, and depletion of hydrocarbon reservoirs (Holzer and Bluntzer, 1984; Galloway et al., 1999). Based on a report conducted by the United States Geological Survey (USGS), land subsidence in Houston-Galveston region continued throughout the 20th century (Stork and Sneed, 2002). Even until recent years, land subsidence of >10 mm/year and up to 25 mm/year is still happening in inland areas north and west of the City of Houston (Yu et al., 2014). Hence, it is important to evaluate flood impacts in regions prone to land subsidence.

To investigate the impacts of land subsidence on inundation, remote sensing observation has been utilized by previous studies. For instance, Shirzaei and Bürgmann (2018) utilized interferometric synthetic aperture radar (InSAR) and global navigation satellite system to

estimate the land subsidence rate in the San Francisco Bay Area and generated the future 100-year inundation maps based on probabilistic projections of sea level rise. Similarly, Catalao et al. (2020) also used InSAR measurements to estimate land subsidence and combined with future sea level rise scenarios to identify the projected flood inundation areas in Singapore. Other than these projection/scenario-based studies, Miller and Shirzaei (2019) analyzed the flood inundation extent of Hurricane Harvey derived from satellite images and correlated it with land subsidence data in two different historical periods estimated from InSAR. Ito et al. (2015) used the digital elevation model (DEM) data obtained from the airborne laser scanning and flood inundation area recorded from the report to examine the relationship between land subsidence and floods in Japan. However, a major limitation by observation-driven approaches is that inundation is often captured via 'snapshots' without fully characterizing its temporal dynamics.

An alternative to remote sensing is to conduct hydrodynamic modeling of flood inundation. Hsu et al. (2010) utilized HEC-RAS 1D and FLO-2D models to analyze the influence of the land subsidence for flood hazards based on two designed flow rates with 1994 and 2004 DEM data. Yin et al. (2013) conducted a scenarios-based study using a 1D/2D coupled flood inundation model to investigate compound effects of land subsidence and sea level rise on fluvial flooding in Shanghai, China. Carisi et al. (2017) investigated the flooding intensity in Italy for four different terrain configurations using a hydrodynamic model which includes both 1D and 2D simulations. Dang et al. (2018) used the hydrodynamic model MIKE 11 to study the impact of land subsidence, sea level rise, and water infrastructure development in Vietnam based on some designed scenarios. Ouyang et al. (2020) applied MIKE models over two periods (before and after land subsidence caused by the Tohoku earthquake) to quantify the effects of land subsidence on the inundation areas in Japan. Hydraulic/hydrodynamic modeling approach provides significant advantages over remote sensing methods due to its ability to capture the

flood dynamics spatially and temporally.

Nonetheless, both remote sensing and hydrodynamic approaches to quantify the effects of land subsidence on flood inundation heavily rely on the surveyed DEM (Hsu et al., 2010; Ito et al., 2015; Carisi et al., 2017; Ouyang et al., 2020), field measurements/monitoring (Miller et al., 2008; Wang et al., 2012; Yin et al., 2013, Yin et al., 2016;), and remote sensing techniques (Dixon et al., 2006; Dang et al., 2018) to represent land subsidence information. The infrequent, short-duration, topology surveys/monitoring inevitably requires assuming a linear land subsidence at some constant rate, which could be unrealistic especially when the anthropogenic activities like groundwater pumping drive the land subsidence. Therefore, few attentions have been paid to quantifying the evolution of land subsidence influence on flood extent and depth over an extended historical period. This is largely due to the lack of reliable methods to realistically estimate land subsidence both continuously and at high spatial resolution.

In addition to land subsidence, many studies have demonstrated that the change of land use/land cover (LULC) has a considerable influence on flood regimes (Li et al., 2018; Hussein et al., 2020). The population of coastal counties in the United States has continuously increased in recent decades with a 39 percent rise (34.8 million people) between 1970 and 2010 (Noori et al., 2016). As human population and economic development have increased, the rate of deforestation, urbanization, and other types of LULC changes has accelerated as well. The changes of LULC can have an impact on hydrological processes by altering evapotranspiration rates, flood peaks, sediment transport rates, concentrations of water quality elements, and a variety of other processes (Eshleman 2004). According to Du et al., 2012, small flooding events are more sensitive to urbanization than large flooding events, the impact of LULC change on peak flow and runoff volume is observed mostly at low intensity and frequent rainfall events. However, exceptional events may still result in higher flows in urbanizing watersheds due to

enhanced hydraulic efficiency (Smith et al. 2002). To check how these changes influence streamflow, the data can be evaluated through field observations or simulation modeling. Since field research is usually expensive and time-consuming, hydrodynamic models are commonly used to estimate or predict the impact of urbanization on streamflow. In general, the impact of urbanization on watersheds has been thoroughly investigated in a number of previous studies and the majority of past studies have focused on how LULC affects flood extent, peak flow and/or surface loss volume (Verbeiren et al. 2013). There is limited research on evaluating the impact of LULC on other flooding aspects like flood depth and velocity together with the impact of land subsidence in historical and future years. Therefore, the study to examine the H&H behavior in order to understand the impact of the land subsidence and LULC is essential. Human activities can significantly impact the flooding characteristics by altering and droughts, which can influence aquatic and terrestrial ecosystems and people's lives and cause significant economic losses. Land subsidence (LS), a destructive worldwide hazard which can be caused by a wide range of anthropogenic and natural factors, is recognized as a serious issue for causing damage to urban and civil infrastructure (Li et al., 2021; Xu et al., 2012; Gambolati and Teatini., 2015; Pérez-Falls et al., 2022). The phenomena might also result in changes on urban flooding (Dixon et al., 2006; Abidin et al., 2015; Yin et al., 2016; Shirzaei and Bürgmann, 2018; Jiang et al, 2023). However, the impact of land subsidence and flooding still has not been fully understood. Most previous studies focused on the general flood hazard, and little attention has been paid to quantifying the land subsidence influence on flood extent, depth and flow velocity at a temporal scale. Though there is some research that assessed flood extent or flood depth resulting from land subsidence. Yet, few attentions have been paid to quantifying the evolution of land subsidence influence on flood extent and depth over an extended historical period (Hsiao et al., 2022; Navarro-Hernández et al., 2022). In addition to land subsidence, the land cover changes due to

8

urbanization is another factor which might influence the flooding (Moe et al., 2017; Li and Bortolot, 2022). To this end, this study is motivated to investigate retrospective change of regional topology due to 145 years (1900 to 2045) of land subsidence and LULC and thus to advance the understanding of the complex interaction between land subsidence, LULC and flood characteristics. Being one of the most destructive natural disasters throughout the world, flood does not only pose a great threat to human beings and their living environment, but also causes severe damage to the economy (Penning-Rowsell et al., 2005; Khan et al., 2010; Michel-Kerjan and Kunreuther, 2011; Kellens et al., 2013; Patel et al., 2017; Farooq et al., 2019; Munawar et al., 2019; Kim et al., 2020; Ahmadlou et al., 2021). Based on the international disaster database, flooding has resulted in a total loss of over $870 billion globally since 1900 (EM-DAT, 2020). In the United States (U.S.) alone, flooding has caused more than $68 billion in loss between 1970 and 2019 (FEMA, 2020). As one of the most devastating events, 2017 Hurricane Harvey (2017) caused severe flooding in coastal Texas, and many records reported that numerous houses damaged during Hurricane Harvey (2017) are located even outside of the 500-year floodplain areas (Jonkman et al., 2018; Miller and Shirzaei, 2019). The unprecedent nature of the Harvey floods calls for a significant advancement in understanding of the processes of determining flood risk and severity.

HEC-RAS has been developed as a software which has capabilities of performing 2D hydrodynamic modeling since 2016 (Brunner, 2016a). HEC-RAS 5.0.7, which was released in March 2019, has the ability to visualize and examine the results in the model itself (Brunner, 2016a). The limitations of HEC-RAS 1D model calculations are compensated by the 2D computing capabilities, resulting in a more precise result of flood inundation with two equation sets in HEC-RAS 5.0.7 to compute 2D flow, which are Diffusion Wave equations and Full Momentum (Saint Venant) equations (Brunner, 2016a and Brunner, 2016b). Being studied and

tested in several cases, it is proved to be an efficient tool on 2D flood simulations (David and Schmalz, 2020; Costabile et al., 2021; Edwards, 2021). Moreover, the newly released HEC-RAS 6.X provides several new features like adding a new 2D solver option, the ability to use spatially and time varying precipitation and infiltration to 2D flow areas, storage areas, and improving the computational speed by further parallelizing the 2D code compared to the previous HEC-RAS 5.0.7. Therefore, the latest version of HEC-RAS 6.3.1 is selected as the tool to perform 2D simulations at the Brays Bayou watershed in this study. Land subsidence, a destructive worldwide hazard which can be caused by a wide range of anthropogenic and natural factors, is recognized as a serious issue for causing damage to urban and civil infrastructure (Li et al., 2021; Xu et al., 2012; Gambolati and Teatini., 2015; Pérez-Falls et al., 2022). The phenomena may also result in changes in urban flooding (Dixon et al., 2006; Abidin et al., 2015; Yin et al., 2016; Shirzaei and Bürgmann, 2018). However, the impact of land subsidence to flooding still has not been fully understood. Most previous studies focused on the general flood hazard, and little attention has been paid to quantifying the land subsidence influence on flood extent, depth and flow velocity at a temporal scale. Though there is some research that assessed flood extent or flood depth resulting from land subsidence. Yet, few attentions have been paid to quantifying the evolution of land subsidence influence on flood extent and depth over an extended historical period (Hsiao et al., 2022; Navarro-Hernández et al., 2022). In addition to land subsidence, the land cover changes due to urbanization is another factor which might influence the flooding (Moe et al., 2017; Li and Bortolot, 2022). To this end, this study is motivated to investigate retrospective change of regional topology due to 145 years (1900 to 2045) of land subsidence and thus to advance the understanding of the complex interaction between land subsidence, land cover and flood characteristics.

Chapter 3: Study Area and Data

3.1 BACKGROUND INTRODUCTION

As one of the most devastating tropical storms, 2017 Hurricane Harvey caused severe flooding and damage in Houston, Texas. Besides enormous rainfall amount, land subsidence might be another contributing factor to the Harvey flood. However, few studies have numerically quantified the evolvement of land subsidence over decades, largely due to the lack of reliable methods to realistically estimate land subsidence both continuously and at high spatial resolution. Therefore, this study aims to investigate retrospective changes of regional topology due to 120 years (1900 to 2045) of land subsidence and the consequent impacts on flood inundation. Based on continuous land subsidence, a series of simulations on the 2017 Hurricane Harvey in Brays Bayou, Texas using a hydrodynamic/hydraulic model is conducted. The results indicate that the overall change of flood depth caused by land subsidence is relatively minor with the flood water deepened by six centimeters per one meter of subsided land at the worst impacted location. The impact from land subsidence on flood depth exhibits strong nonlinearity in time, where effects from previous land subsidence hotspots could be altered by later continuing land subsidence. Spatially, change in flood depth due to the land subsidence is not only heterogeneous but mixed with coexisting increased and reduced flood depths. The results of this study improve the understanding of the dynamic evolvement of flood inundation due to continuous land subsidence so that better planning can be initiated for sustainable urban development for coastal communities, which is imperative under ongoing climate change and sea level rise.

This study investigates retrospective changes of regional topology due to 145 years (1900 to 2045) of land subsidence, which is enabled by a high-resolution, physics-based modeling of groundwater withdrawal and the consequent aquifer-system compaction. By analyzing the spatial

heterogeneity of land subsidence and the consequent change over flood inundation using a hydrodynamic model in different historical periods, we have an unprecedented chance to better understand the complex of flood inundation and its relationship with land subsidence. The outcome of this study can help people better understand the dynamic evolvement of flood inundation due to land subsidence so that better planning can be initiated for sustainable urban development for coastal communities. Research objectives of this study are (1) to examine the change in topology due to a historical 145-year land subsidence, (2) to establish a hydrodynamic model that accurately reproduces the flood inundation of 2017 Hurricane Harvey, and (3) to investigate the change in Harvey flood inundation due to the historical land subsidence in Brays Bayou, Texas.

3.2 STUDY AREA

Harris County, located in the southeastern of Texas (**Fig. 1a**), has experienced tremendous increases in development in the past decades (Walker and Shelton, 2016; Chun et al., 2021). Owing to the rapid growth and groundwater withdrawal, land subsidence in this region has been occurring for years (Kasmarek et al., 2009) and **Fig. 1a** shows the cumulative land subsidence simulated using the Houston Area Groundwater Model (HAGM, Kasmarek, 2013) from 1900 to 2017 in this region. Not only has the increased urbanization caused subsidence, but it also has aggravated this region's flood vulnerability (Garcia et al., 2020). From 1996 to 2019, there are over one hundred flood events that occurred in Harris County (FEMA), with about 10.3 billion US dollars of the total estimated losses to property damage (NOAA, 2020).
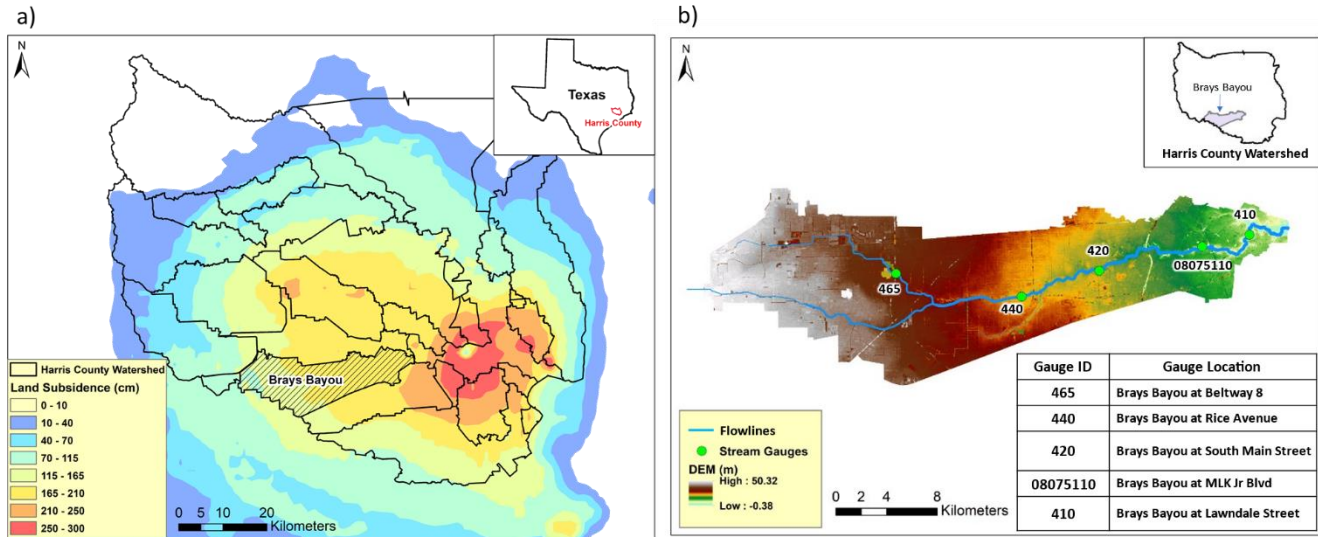
Figure 1: Land use and land cover in Brays Bayou from the National Land Cover Database.

Located close to the land subsidence center (**Fig. 1a**), the Brays Bayou watershed is selected as the study area with a drainage area of approximately 330 km2. 95 % of Brays Bayou is developed land (**Fig. 2**) and it is one of the most urbanized watersheds in Harris County (Bass, 2017; Gao et al., 2021). The climatology in this region is wet and subtropical with humid, hot summers and mild winters (Li et al., 2021). This area is vulnerable to floods due to its flat terrain, impermeable land surface (**Fig. 3**), clayey soil (**Fig. 4**), and frequent, extreme rainfall from tropical storms and hurricanes (Bedient et al., 2003; Bass et al., 2017; Li et al., 2021). Previous studies have shown that land subsidence made the overland and channel slopes flatter than 0.001 % downstream from Main Street to the East in Brays Bayou (Vieux and Bedient, 2004). **Fig. 1b** shows the Brays Bayou watershed with the digital elevation model (DEM) and five stream gauges.
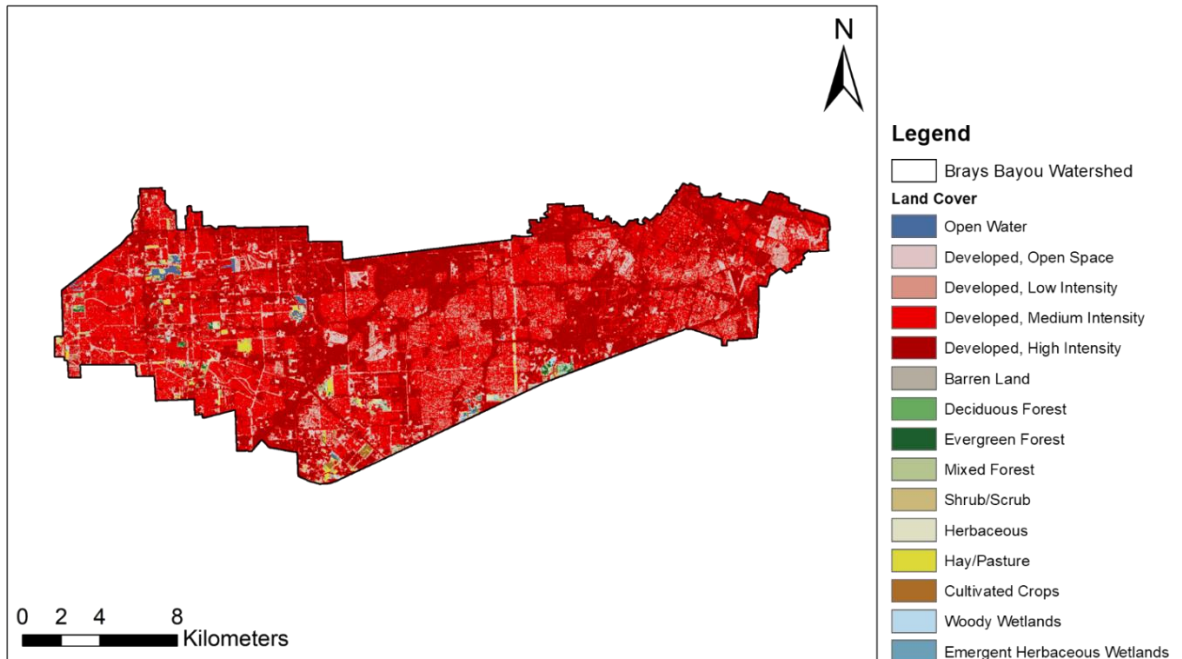
Figure 2: Land use and land cover in Brays Bayou from the National Land Cover Database.
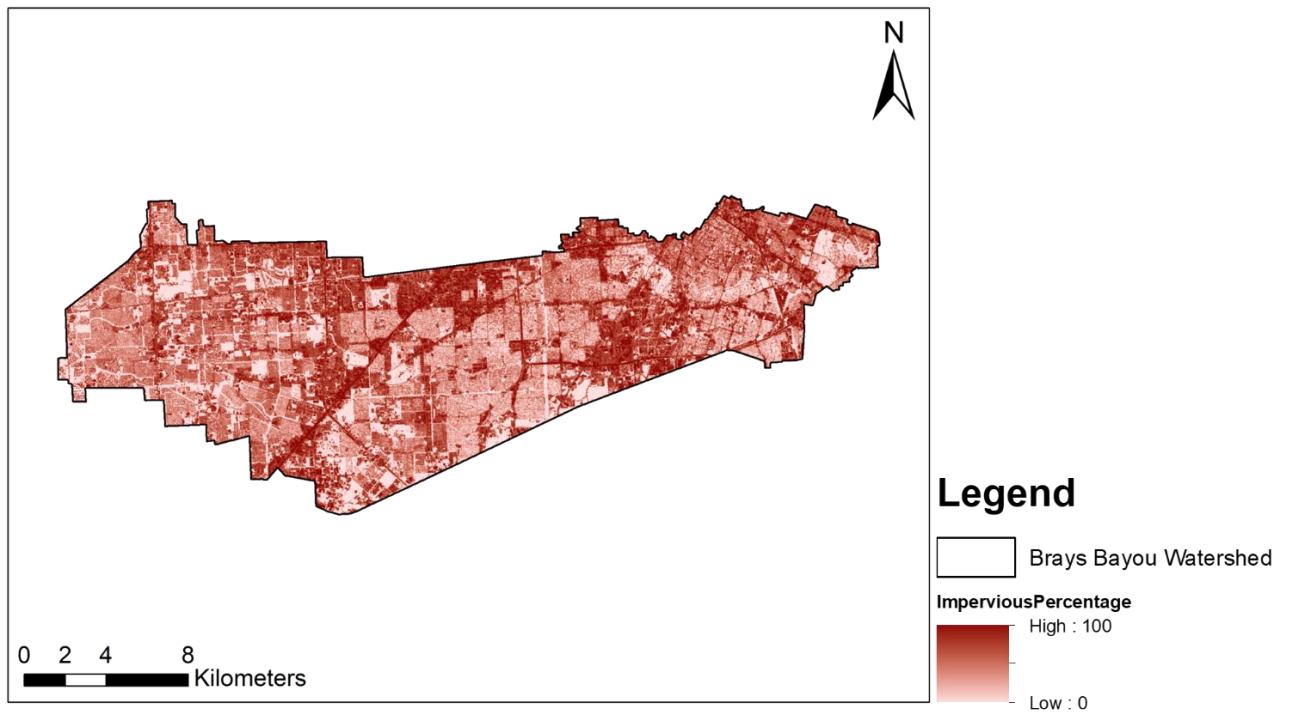
Figure 3: Imperviousness in Brays Bayou from the National Land Cover Database.
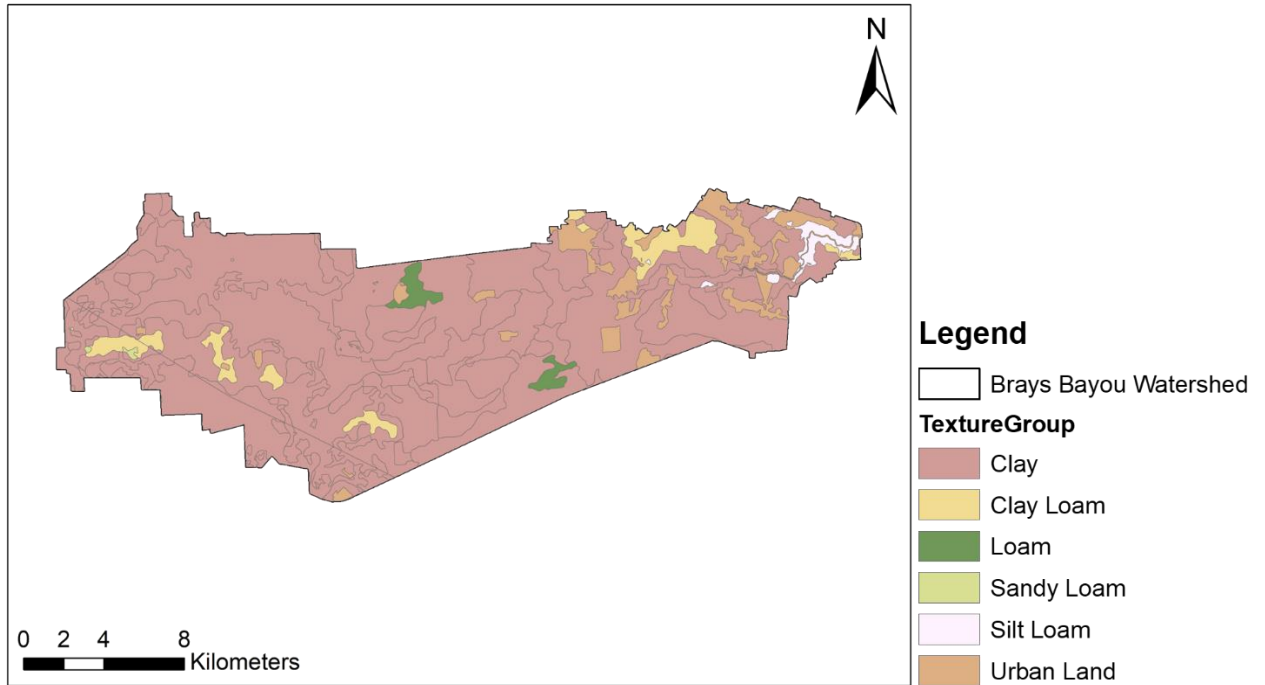
Figure 4: Soil type in Brays Bayou from the gridded National Soil Survey Geographic Database.

3.3 DATA

3.3.1 Land subsidence and topography data

In this study, land subsidence caused by groundwater withdrawal is simulated using the Houston Area Groundwater Model (HAGM) updated by Kasmarek (2013) with the Subsidence and Aquifer-System Compaction (SUB) package (Hoffmann et al., 2003). HAGM simulates groundwater flow and land subsidence in the northern part of the Gulf Coast aquifer system in Texas from predevelopment (before 1891) through 2009. Land subsidence from 2009 to 2017 is simulated with HAGM by using the 2009 groundwater pumping plan of a total 3 m^3/day since no significant primary compaction subsidence was observed during the stable groundwater level period in trend for the Chicot and Evangeline aquifers (Liu et al., 2019). As much as 3.05 meters of land subsidence was observed in 1979 in the Houston-Galveston region as a result of inelastic compaction of aquitards in the Chicot and Evangeline aquifers between 1937 and 1979 (Galloway et al., 1999) and simulated subsidence up to 3.0 meter (300 cm) can be found in **Figure 1a**.

The spatial and temporal distribution of land subsidence rates from 1900 to 2045 in the Brays Bayou watershed can be seen in **Figures 5a**-**5h**. No significant subsidence is found for the period of 1900 to 1930 in the study area (**Figure 5a**). Then the pre-consolidation pressure heads within the Chicot and Evangeline aquifers continuously reacted to lowering groundwater levels, which in turn was caused by continuously increasing groundwater withdrawal rates from 0.57 to 4.28 million m^3/day by 1979 (Liu et al., 2019). **Figures 5b**, **5c** and **5d** show simulated subsidence rates up to 40 to 55 mm/year in a small border area during 1930 to 1960, up to 40 to 55 mm/year in an extended area during 1960 to 1970, and up to 75 to 95 mm/year in a big central area during 1970 to 1980. This land subsidence occurred without any management over

groundwater levels before 1979. However, it is found that the management of recovering groundwater levels from 1979 to 2000 successfully decreased inelastic primary compaction from up to 79 to 95 mm/year during 1970 to 1980 (**Figure 5d**) down to up to 40 to 55 mm/year during 1980 to 1990 (**Figure 5e**) and further down to less than 5 mm/year with some land rebound (less than zero mm/year) during 1990 to 2045 (**Figure 5f**, **5g** and **5h**) through decreasing groundwater withdrawals from 4.3 to 3.0 million m^3/day as shown in Appendix **Figure A4**. Land subsidence rates of 0.08 to 8.49 mm/year since 2005 observed by 13 borehole extensometers is due to creep compaction of the Gulf Coast aquifer system (Liu et al., 2019), which is out of simulated subsidence only due to groundwater pumping (Kasmarek, 2013). Overall, land subsidence increases rapidly, especially from 1960 to 1970 with the mean areal rate of 38.2 mm/year and from 1970 to 1980 with the mean areal rate of 58.8 mm/year. Then the land subsidence rate almost stopped increasing after 1980 and ended with the rate of 1.9 mm/year during the period of 2017 to 2045.
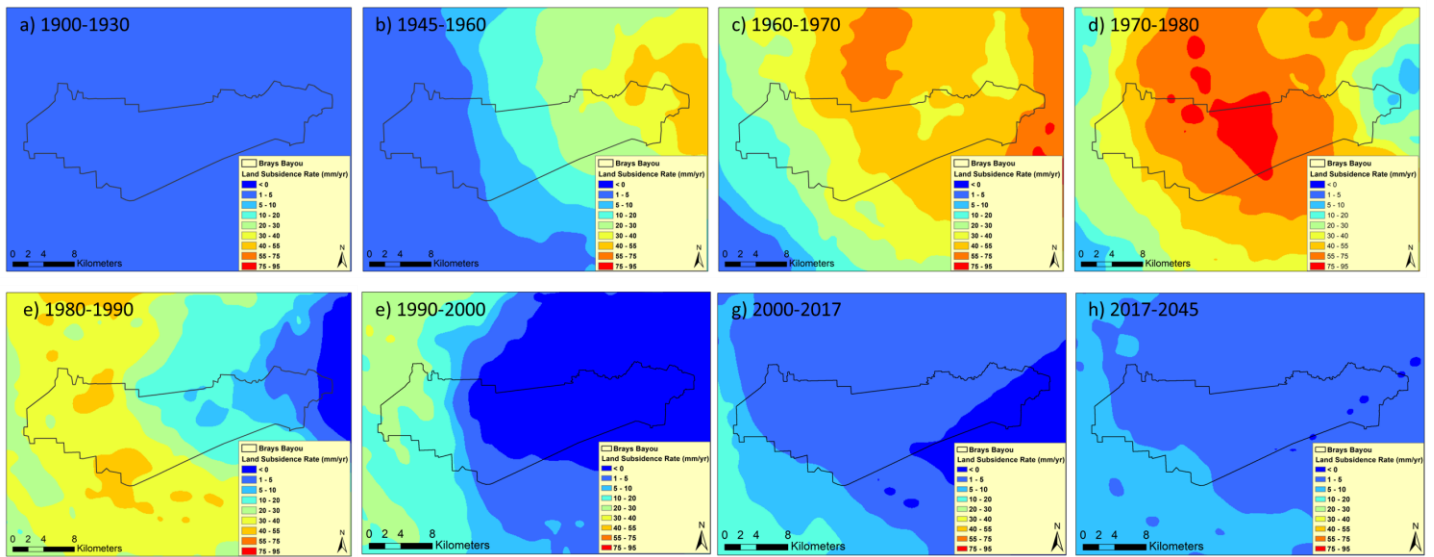
Figure 5: Average annual land subsidence rates during (a) 1900 to 1930, (b) 1930 to 1960, (c) 1960 to 1970, (d) 1970 to 1980, (e) 1980 to 1990, (f) 1990 to 2000, (g) 2000 to 2017, and (h) 2017 to 2045. These rates are calculated based on the simulated land subsidence using the Houston Area Groundwater Model (HAGM).

DEM with 10-m spatial resolution is obtained from the USGS website (https://apps.nationalmap.gov/downloader/#/). Since DEM cannot represent sufficient information on channel cross-sections, bathymetry data needs to be combined with DEM if available to better represent channel shape (Goodell, 2014). In this study, channel bathymetry data is obtained from the Model and Map Management (M3) system (HCFCD, 2020a).

3.3.2   Land use and land cover data

LULC data used in this research are derived from Timelapse imagery from Google Earth Pro, National Land Cover Database (NLCD) and Houston-Galveston Area Council (H-GAC). For 1944, 1953 and 1978, the time-lapse feature to access past imagery for the three years epochs in Google Earth Pro is utilized and the images are exported and converted to raster files in ArcGIS and shown in **Figure 6**. There is information missing at the southwest and east section of the study area in 1944 and 1953, thus assumptions are made in those two areas to generate LULC

18

maps for the whole Brays Bayou Watershed.

Figure 6: Timelapse Image from Google Earth Pro in the time of year (a) 1944, (b) 1953 and (c) 1978

LULC classifications using the manual supervised classification method and the polygon tool are conducted to quantitatively estimate the changes in the LULC. The LULC maps of 1944, 1953 and 1978 are classified into four categories (crop, impervious surface, soil and tree) using supervised method in the image classification tool in ArcGIS. The supervised LULC map of 1944, 1953 and 1978 are shown in **Figure 7**. From 1944 to 1978, the area of impervious area has increased from 4.96% to 18.95% and the area of trees has decreased from 6.71% to 5.30% with increasing urbanization.
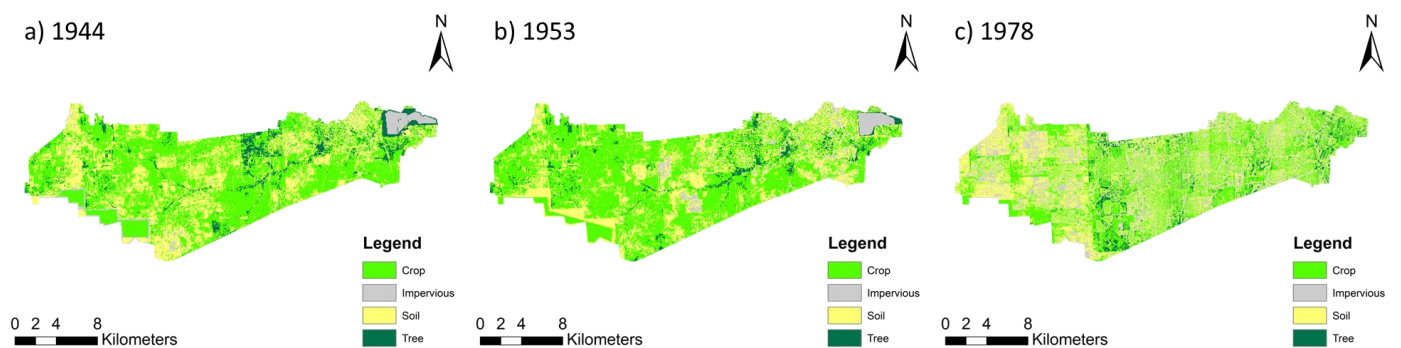
Figure 7: Timelapse Image from Google Earth Pro in the time of year (a) 1944, (b) 1953 and (c)

1978

The land cover data of 1992, 2001 and 2016 is extracted from NLCD and the 2045 data is obtained from H-GAC. Since the land use classes from H-HAC are different from the ones in NLCD, the 10 classes of the H-GAD land use data are further recategorized into 15 classes for conducting the comparison and assessment. The LULC maps of 1992, 2001, 2016 and 2045 are demonstrated in **Figure 8**. It can be seen that in 1992, 82.40% of the watershed is developed area (including open space, low, medium and high intensity). This proportion increased to 95.95%, 96.77 and 99.97% in 2001, 2016 and 2034, respectively. The impervious area from 1992 to 2045 is calculated from the developed areas using different ratios from the classification description from NLCD. The areal coverage and percentage of the LULC types for 1944, 1953, 1978, 1992, 2001, 2016 and 2045 are summarized in **Table 1**.
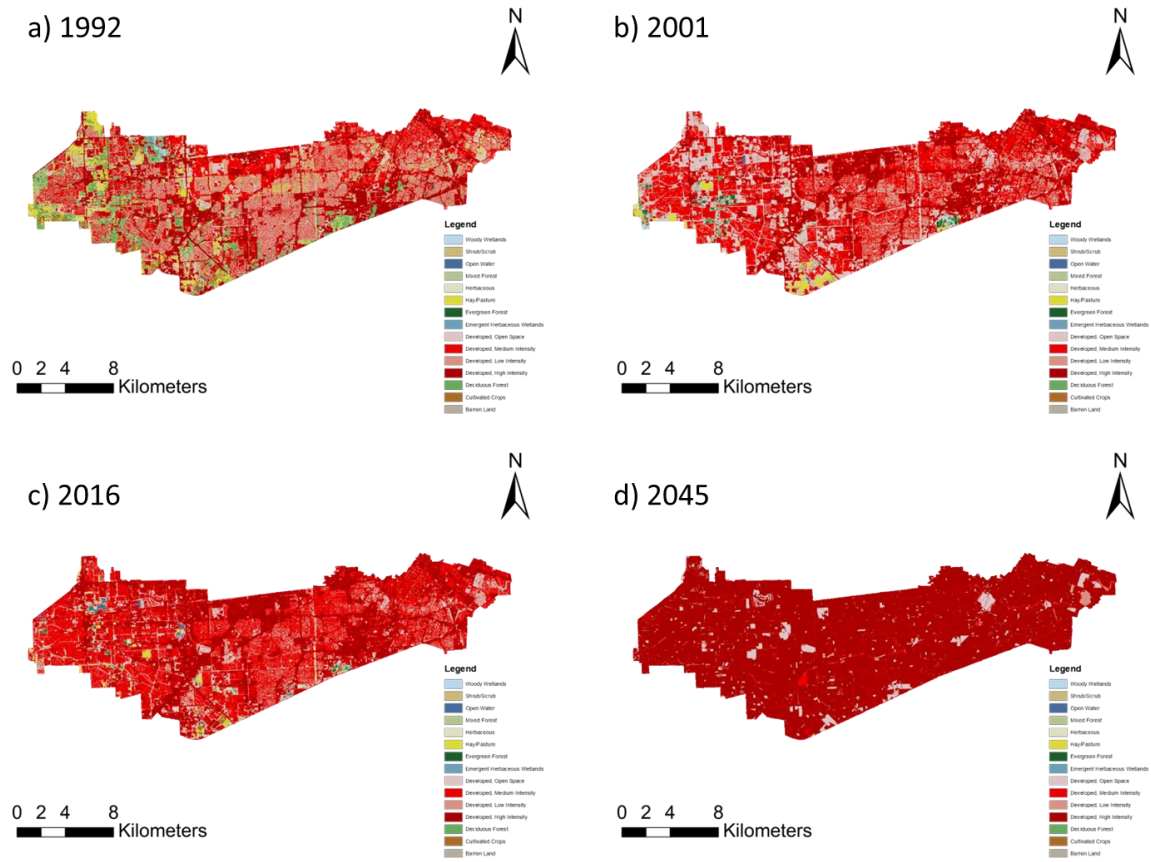
Figure 8: Land cover from NLCD in the time of (a) 1992, (b) 2001, (c) 2016, and (d) 2045.

Table 1: Percentage of LULC Classes at different years

Land Cover Classes	Year										
	1944	1953	1978	1992		2001		2016		2045	
Open Water	-	-	-	0.07%		0.09%		0.39%		0.01%	
Developed, Open Space	Impervious 4.96%	Impervious 6.13%	Impervious 18.95%	6.38%	82.40% Developed Areas	14.28%	95.95% Developed Areas	5.03%	96.77% Developed Areas	4.74%	99.97% Developed Areas
Developed, Low Intensity				29.21%		19.86%		14.48%		1.64%	
Developed, Medium Intensity				25.50%		40.54%		45.13%		3.80%	
Developed, High Intensity				21.31%		21.27%		32.13%		89.79%	
Barren Land	Soil 31.61%	Soil 29.55%	Soil 37.76%	0.17%		0.12%		0.08%		0.00%	
Deciduous Forest	Tree 6.71%	Tree 4.71%	Tree 5.30%	6.58%		0.58%		0.12%		0.00%	
Evergreen Forest				0.22%		0.64%		0.21%		0.01%	
Mixed Forest				1.34%		0.08%		0.19%		0.00%	
Shrub/Scrub	-	-	-	0.35%		0.26%		0.27%		0.00%	
Herbaceous	-	-	-	0.49%		0.66%		0.53%		0.00%	
Hay/Pasture	-	-	-	6.93%		1.21%		0.96%		0.00%	
Cultivated Crops	Crop 56.71%	Crop 59.61%	Crop 37.99%	1.05%		0.10%		0.24%		0.00%	
Woody Wetlands	-	-	-	0.20%		0.29%		0.16%		0.00%	
Emergent Herbaceous Wetlands	-	-	-	0.18%		0.02%		0.05%		0.00%	
Sum	100%	100%	100%	100%		100%		100%		100%	

3.3.3 *Precipitation and observation data*

Precipitation data used in this study is the hourly Stage IV product with 4-km spatial resolution obtained from the National Centers for Environmental Prediction (NCEP), which combines multi-sensor (quality-controlled radar, satellite, and rain gauge) precipitation estimates (Lin and Mitchell, 2005; Habib et al., 2009; Nelson et al., 2016). The Stage IV radar data during Hurricane Harvey have been systematically validated by Gao et al. (2021) and showed close match with ground truths from a dense rain-gauge network.

Observational stage hydrographs at five (5) stream gauges (**Fig. 1b**) are retrieved from the Harris County Flood Warning System website (HCFCD, 2020b). Except the most downstream gauge which is used as the downstream boundary condition for the hydrodynamic model, the rest four stream gauges are utilized as benchmarks to calibrate the model in this study. Ninety-nine (99) highwater marks surveyed during the 2017 Hurricane Harvey are obtained from the Harris County Flood Control District (HCFCD, 2020c) and this information is used to validate the model simulation.

Chapter 4: Methodologies and Results

4.1 Methodologies

4.1.1 Terrain data preparation

Since the year of 2017 is selected as the starting point, the 2017 terrain data is developed by combining the DEM of 2017 with channel bathymetry in RAS Mapper. Then terrain data of other years (1900, 1930, 1945, 1960, 1970, 1980, 1990, 2000, 2010) are developed using the projected land subsidence of that year superimposed upon the 2017 condition as shown in Eq. (1) below:

$$T_Y = T_{2017} + LS_{Y-2017} \tag{1}$$

where T means Terrain, LS is Land Subsidence, and Y is year.

4.1.2 Model set-up, calibration, and simulation scenarios

In this study, the Hydrologic Engineering Center-River Analysis System 2D (HEC-RAS version 5.0.7) is utilized as a modeling tool to simulate the flood inundation due to its broad applications in both industry and academia fields (e.g., Tayefi et al., 2007; Shustikova et al., 2019; Costabile et al., 2020; Ongdas et al., 2020; Shrestha et al., 2020; Karim et al., 2021). **Figure 9** illustrates the input data and workflow of the model set-up and simulations.
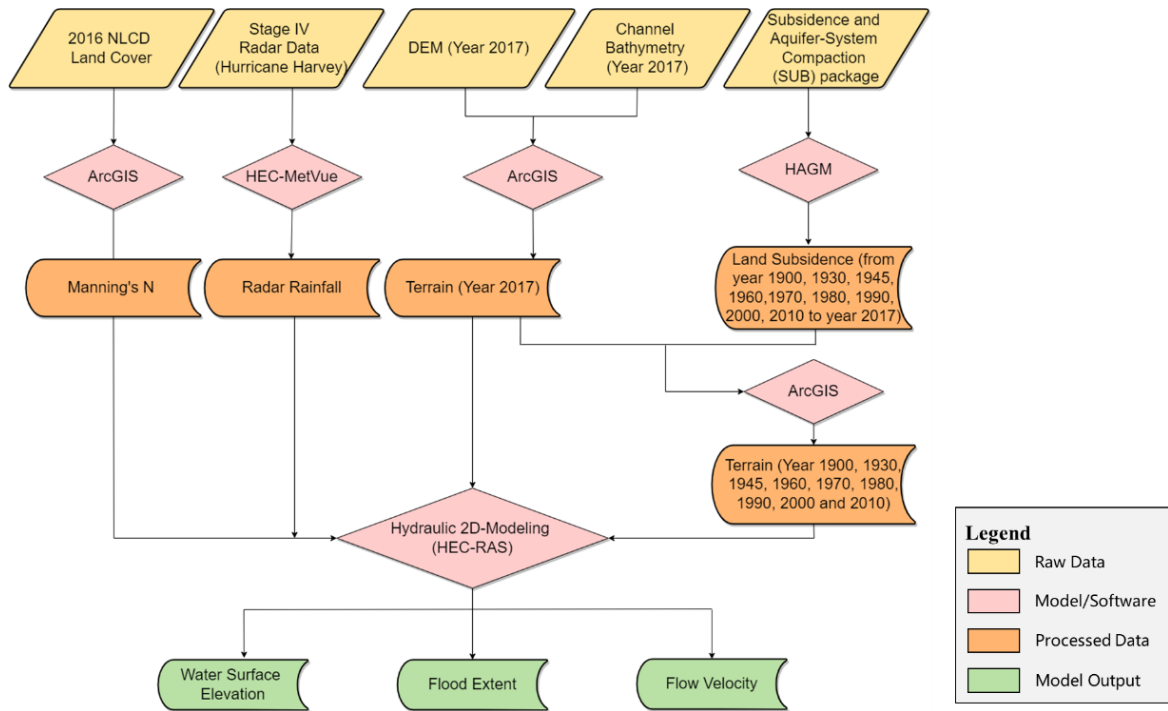
Figure 9: Overarching flowchart of model set-up and simulations

The HEC-RAS 2D model is built by first importing the prepared terrain data (DEM combined with channel bathymetry) into the RAS Mapper. A 2D flow area with grid dimensions of 30-m $\times$ 30-m is then created as a computational mesh, and this cell size is selected in respect to computation time and model stability. The Manning's roughness is assigned based on the land use and land cover data from the 2016 National Land Cover Database (NLCD, https://www.mrlc.gov).

To provide precipitation input, we process the hourly Stage IV rainfall by calculating the areal average values over the watershed (**Fig. 10a**) since the HEC-RAS (version 5.0) only accepts a time series of spatially uniform precipitation as input. The total rainfall from Harvey (Fig. 6) shows little spatial variability with the coefficient of variation being 0.05 for Stage IV rainfall values within the watershed boundary. Therefore, we consider it acceptable to adopt the watershed-averaged precipitation for HEC-RAS input. Another limitation of HEC-RAS v 5.0 is

the inability to represent infiltration. For Hurricane Harvey, Gao et al. (2021) estimated the runoff coefficient in Brays Bayou to be 91 % based the runoff volume received by the most downstream USGS gauge and total rainfall, which is largely due to the 95 % urbanization rate and 72 % imperviousness of Brays Bayou as well as the enormous rain volume from Hurricane Harvey. Given the high runoff coefficient, neglecting loss caused by infiltration and interception is also considered reasonable in this study.
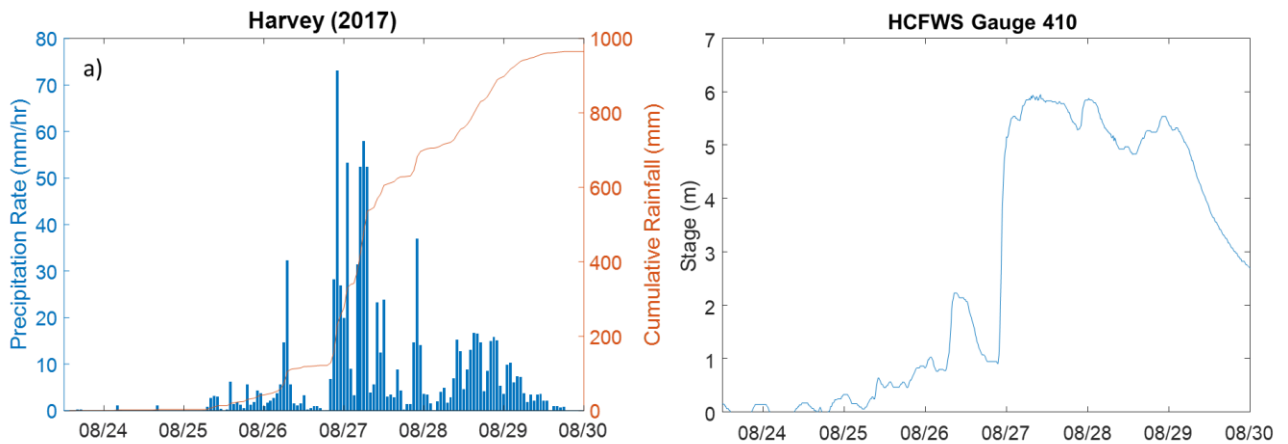
Figure 10: (a) Hyetograph of the mean areal precipitation for the Brays Bayou watershed, and (b) Stage hydrograph at Gauge 410

The stage hydrograph, as shown in **Fig. 10b** at gauge 410 (**Fig. 1b**), is utilized as the downstream boundary condition for the unsteady simulation. Additionally, an initial condition with ramp-up option is set in order to let the flow go through the 2D area and establish the initial wet conditions before the beginning of the simulations. Detailed model specification can be found in **Table 2**.

Table 2: HEC-RAS 2D model settings

Parameters	Settings
Boundary Conditions	Rainfall and downstream stage hydrograph
2D Flow Equation Set	Diffusion Wave
Maximum Iterations	20
Initial Conditions Ramp Up Time (hrs)	120
Boundary Conditions Ramp Up Fraction	0.5
Model Computation Interval	3-min
Model Output Interval	15-min

To consider the land subsidence, the authors build respective HEC-RAS 2D models to represent the corresponding topography from 1900 to 2017 through modifications of terrain data. The model of 2017 is manually calibrated for Hurricane Harvey (8/25/2017-8/30/2017) by comparing the simulated and observed stage hydrographs at four-gauge locations (gauges 465, 440, 420, and 08075110). The Manning's roughness coefficients are modified via a uniform multiplicative factor during the calibration process. Once the calibration is satisfactory, we use 99 surveyed highwater marks during Hurricane Harvey to validate the calibration results. After the model calibration and validation, the optimized Manning's roughness is implemented for models of other years between 1900 and 2017. Thus, each simulation scenario has the same model settings except the associated terrain to represent only the impacts caused by the land subsidence.

4.1.3 Quantitative statistics

Calibration results are evaluated using the root mean squared error (RMSE), Nash-Sutcliffe Efficiency (NSE), and correlation coefficient (CC). RMSE describes the discrepancy between the simulation and observation, quantifying the scale of the error (Mediero et al., 2011). The closer the RMSE value to 0, the more accurate the model is. While NSE shows how well the plot of observation results versus the simulation fits the 1:1 diagonal line. The higher NSE value

is, the better the simulation performance (Legates and McCabe, 1999). CC measures the linear correlation between simulation and observation. Because in this study we intend to analyze the maximum flood inundation, the absolute error at the flood peak timing is evaluated. The equations of computing RMSE, NSE, CC, and absolute error at peak timing are shown in Eqs. (2), (3), (4), (5):

$$RMSE = \sqrt{\frac{\sum_{i=1}^{n}(H_{sim}^{i}-H_{obs}^{i})^{2}}{n}} \qquad (2)$$

$$NSE = 1 - \frac{\sum_{i=1}^{n}(H_{sim}^{i}-H_{obs}^{i})^{2}}{\sum_{i=1}^{n}(H_{obs}^{i}-\overline{H_{obs}})^{2}} \qquad (3)$$

$$CC = \frac{1}{n-1}\sum_{i=1}^{n}(\frac{H_{sim}^{i}-\mu_{sim}}{\sigma_{sim}})(\frac{H_{obs}^{i}-\mu_{obs}}{\sigma_{obs}}) \qquad (4)$$

$$Absolute\ Error = \left|H_{sim}^{peak} - H_{obs}^{peak}\right| \qquad (5)$$

where H_{sim}^{i} is the simulated flood depth of the ith data, H_{obs}^{i} is the observed flood depth of the ith data, and $\overline{H_{obs}}$ is the mean of the observed flood depth. μ_{sim} and σ_{sim} are the mean and standard deviation of simulated data, respectively. μ_{obs} and σ_{obs} are those of observation, and n is number of the total data points.

To compare the changes in maximum flood depth caused by the land subsidence, the authors calculate the flood depth difference (FDD) by subtracting the maximum flood depth simulated using the scenario for 1900 from the maximum flood depth simulated from other years (e,g, year Y). Since the 1900 scenario is the baseline flood condition without land subsidence, the subtrahend is always the maximum flood depth in the Year 1900 for this quantification, as shown in Eq. (6) below:

$$FDD = D_{sim}^{Y} - D_{ref}^{1900} \tag{6}$$

where D_{sim}^{Y} is the simulated flood depth in year Y and D_{ref}^{1900} is the reference flood depth in 1900. The positive FDD means the maximum flood depth in year Y is deeper than the baseline condition (1900), indicating the adverse impacts caused by the land subsidence between 1900 and year Y. A negative value of FDD means the maximum flood depth in year Y is smaller than the year 1900.

After simulating all scenarios, two indices are calculated to analyze the temporal difference in flood inundation results, which are Fit Statistic and Root Mean Square Deviation (RMSD). The Fit Statistic exhibits the inundated areas of simulation as a fraction of the reference, which represents a meaningful assessment of the inundation extents (Bates and De Roo, 2000; Yin et al., 2016; Rajib et al., 2020). The metric is calculated as follows:

$$Fit = \frac{A_o}{A_r + A_s - A_o} \tag{7}$$

where A_o refers to the overlapped inundated area of the reference and simulation, A_r refers to the reference inundated area (in this case the reference is the inundated area in 1900) and A_s refers to area of simulated flood extent. The Fit index ranges from 0 if none of the simulated areas matches the reference to 1 for a perfect fit.

The RMSD compares flood depth between simulated results and the reference upon a cell-by-cell basis (Yu and Lane, 2011; Grimaldi et al., 2019). It is calculated as in the following Eq. (8):

$$RMSD\ (depth) = \sqrt{\frac{\sum_{i=0}^{n}(D_{sim}^{i} - D_{ref}^{i})^2}{n}} \tag{8}$$

where D_{sim}^{i} and D_{ref}^{i} are the simulated and reference flood depth of the ith cell, and n is the

number of inundated cells.

4.1.4 Evaluation Scenarios

To evaluate and comprehend the effect of the land subsidence and LULC on flood characteristics, three scenarios (S1, S2, and S3) are designed to be evaluated with different combinations that illustrate the land subsidence conditions from 1900 to 2045, LULC conditions from 1944 to 2045 and rainfall conditions from 1944 to 2045, respectively. For example, the first scenario (S1) is executed using the terrain from different years, 2017 LULC and 2017 rainfall, representing the impact from the land subsidence alone. The second scenario (S2) allows to observe and compare the changes in flood characteristics in each scenario due to the impact of land LULC changes alone. And the third scenario represents the compound impact of land subsidence and LULC. The scenarios are summarized in **Table 3**.

Table 3: Three scenarios for HEC-RAS 2D simulation

Scenarios	Simulation ID	Land Subsidence	Urbanization (Manning's N)	Rainfall (Imperviousness)
S1 (Impact from Terrain only)	1	1900	2017	2017
	2	1945	2017	2017
	3	1953	2017	2017
	4	1978	2017	2017
	5	1992	2017	2017
	6	2001	2017	2017
	7	2017	2017	2017
	8	2045	2017	2017
S2 (Impact from Urbanization)	1	2017	1944	1944
	2	2017	1953	1953
	3	2017	1978	1978
	4	2017	1992	1992
	5	2017	2001	2001
	6	2017	2017	2017
	7	2017	2045	2045
S3 (Impact from both Terrain and Urbanization)	1	1945	1944	1944
	2	1953	1953	1953
	3	1978	1978	1978
	4	1992	1992	1992
	5	2001	2001	2001
	6	2017	2017	2017
	7	2045	2045	2045

4.2 Results

4.2.1 Model calibration and validation

The calibration results for Hurricane Harvey (**Table 4**) show a good fit between the simulated and observed with CC larger than 0.9 and NSE higher than 0.8 at four gauges. The comparisons of stage hydrographs can be found in **Figure 11**.

Table 4: Statistics of calibration results at four stream gauges along Brays Bayou

Gauge ID	RMSE (m)	NSE	CC	Absolute Error at Peak Timing (m)
465	0.87	0.84	0.95	0.28
440	1.11	0.81	0.90	0.44
420	0.99	0.87	0.94	0.40
08075110	1.07	0.88	0.94	0.36
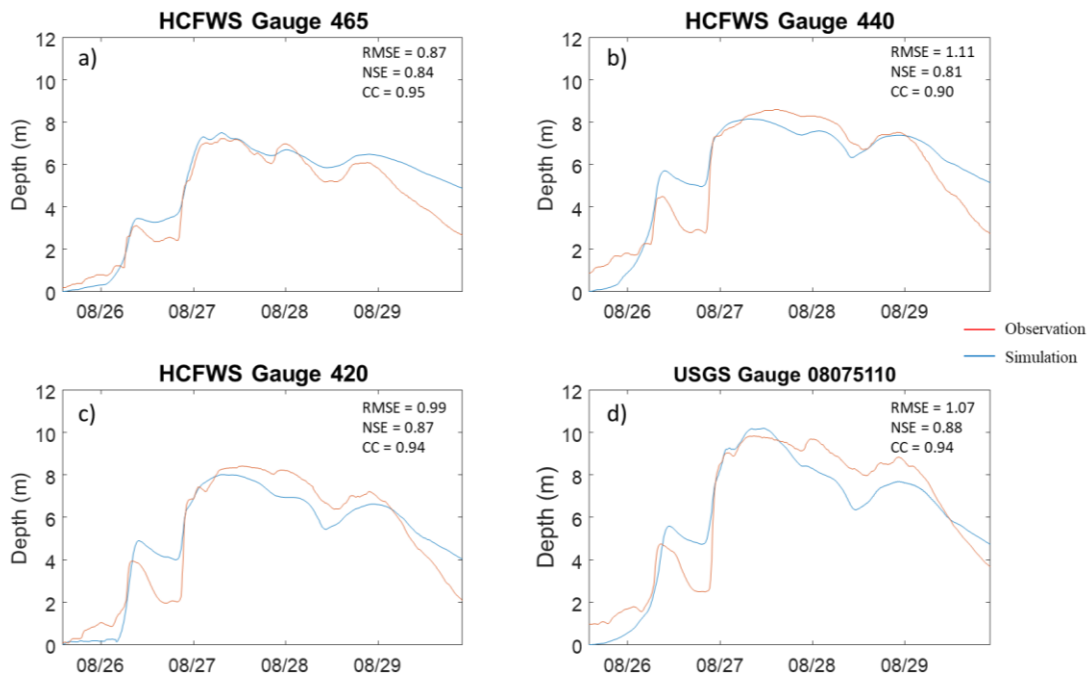
Figure 11: Calibration results of the stage hydrographs for Hurricane Harvey at (a) Gauge 465, (b)

Fig. 12a shows the locations of the surveyed highwater marks used for validation. The comparison between the observed and simulated is presented in **Fig. 12b**. Overall, the correlation of determination of 0.95 between the simulated flood depths and highwater marks indicates that the model is reliable to reproduce the flood depth well and allows us to further investigate the impacts of land subsidence on flood inundation.
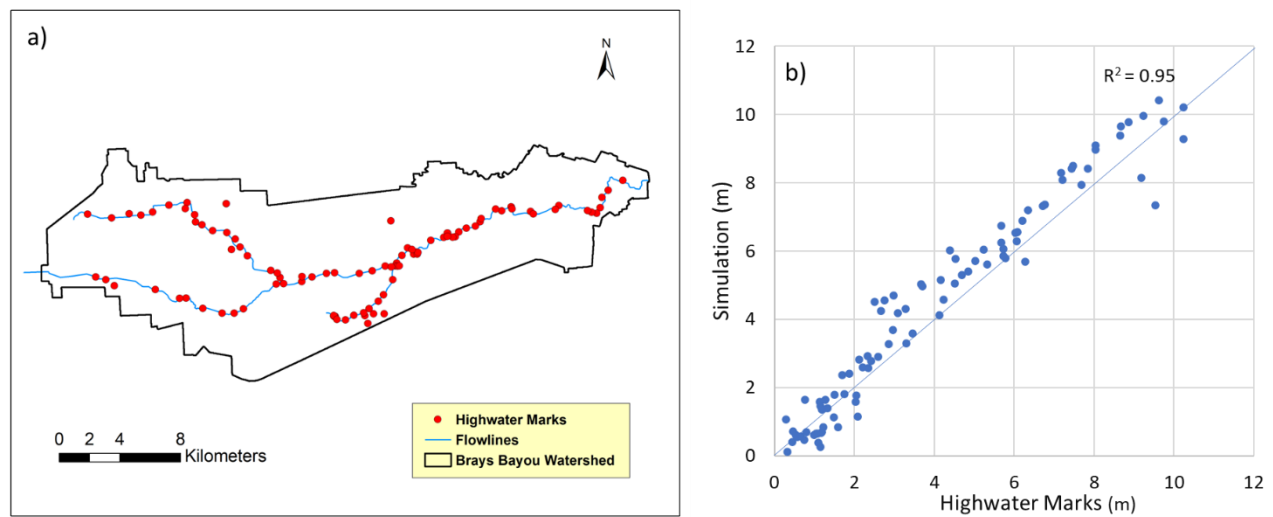
Figure 12: Highwater marks in the Brays Bayou watershed and (b) Comparison of the surveyed and simulated water depth of Hurricane Harvey

4.1   Spatial-temporal patterns of maximum flood extent and depth

Examining the spatial and temporal patterns of the maximum flood extent and flood depth allows the authors to identify varying degrees of the impacts of land subsidence on flood inundation in the study area. The simulated results from the calibrated HEC-RAS 2D model for the maximum flood depth based on the topography of 1900 and 2017 are shown in **Fig. 13a** and **b**, respectively. To decipher the changes of the corresponding flood inundation with respect to the impacts from the land subsidence, the authors calculate the flood depth difference (FDD)

between 2017 and 1900 (**Fig. 13c**), alongside land subsidence contours for the corresponding years (**Fig. 13d**). Overall, the spatial patterns of changes in flood depth are found to be consistent with land subsidence. For example, compared to the simulated flood depth under the 1900 condition, the areas within Zones A and B are observed with much deeper water under the 2017 condition, which coincides with the higher subsidence found locally in those areas (Zones A and B).
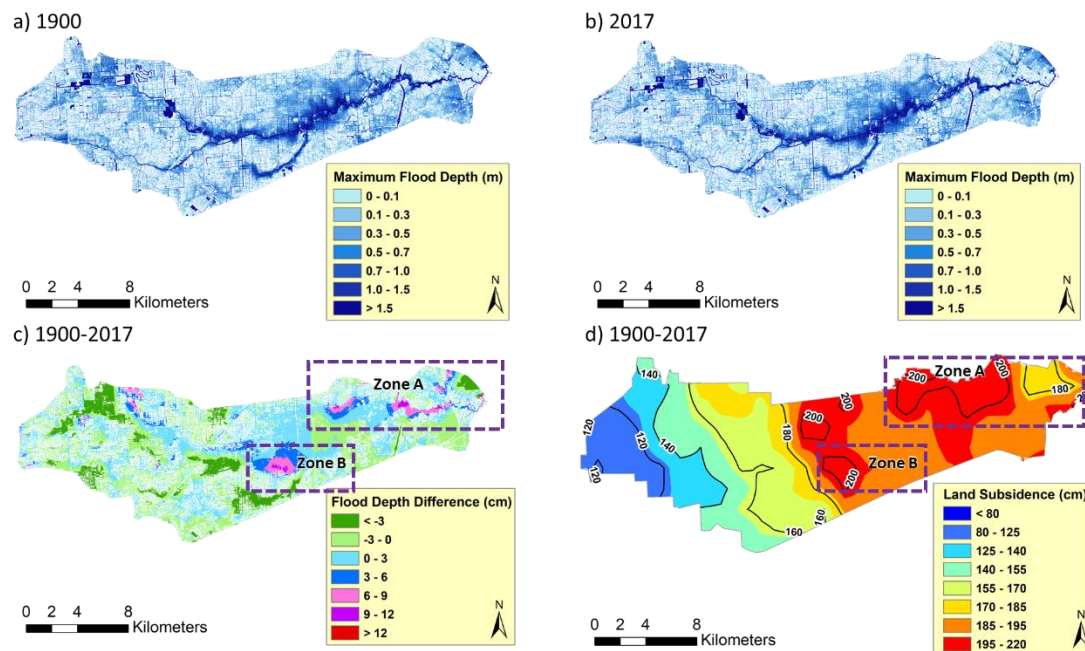
Figure 13: (a) Maximum flood depth in1900, (b) Maximum flood depth in 2017, (c) Flood depth difference (FDD) between 1900 and 2017, and (d) Land subsidence contours in the period of 1900 to 2017

In addition, the spatial differences in maximum flood depth between the baseline condition (1900) and the subsequent years (1960, 1970, 1980, 1990 and 2045) for Hurricane Harvey are also calculated, as shown in **Figs. 14a** to **h**. The substantial changes in flood depth

can be identified near the subsidence centers (labeled as Zone A in **Figs. 14a** to h, Zone B in **Fig. 14e** to h) for various time periods. From the time-series of change in land subsidence, as shown in **Fig. 14b**, **d**, **f**, and **h**, one can see that the land subsidence started from the downstream to upstream sections of the watershed with non-uniform subsidence rates. It is found that the changes in flood depth within Zone B became significant after 1980 (**Fig. 14e** and **g**), which corresponds well with the larger land subsidence occurring in midstream (**Fig. 14f** and **h**).
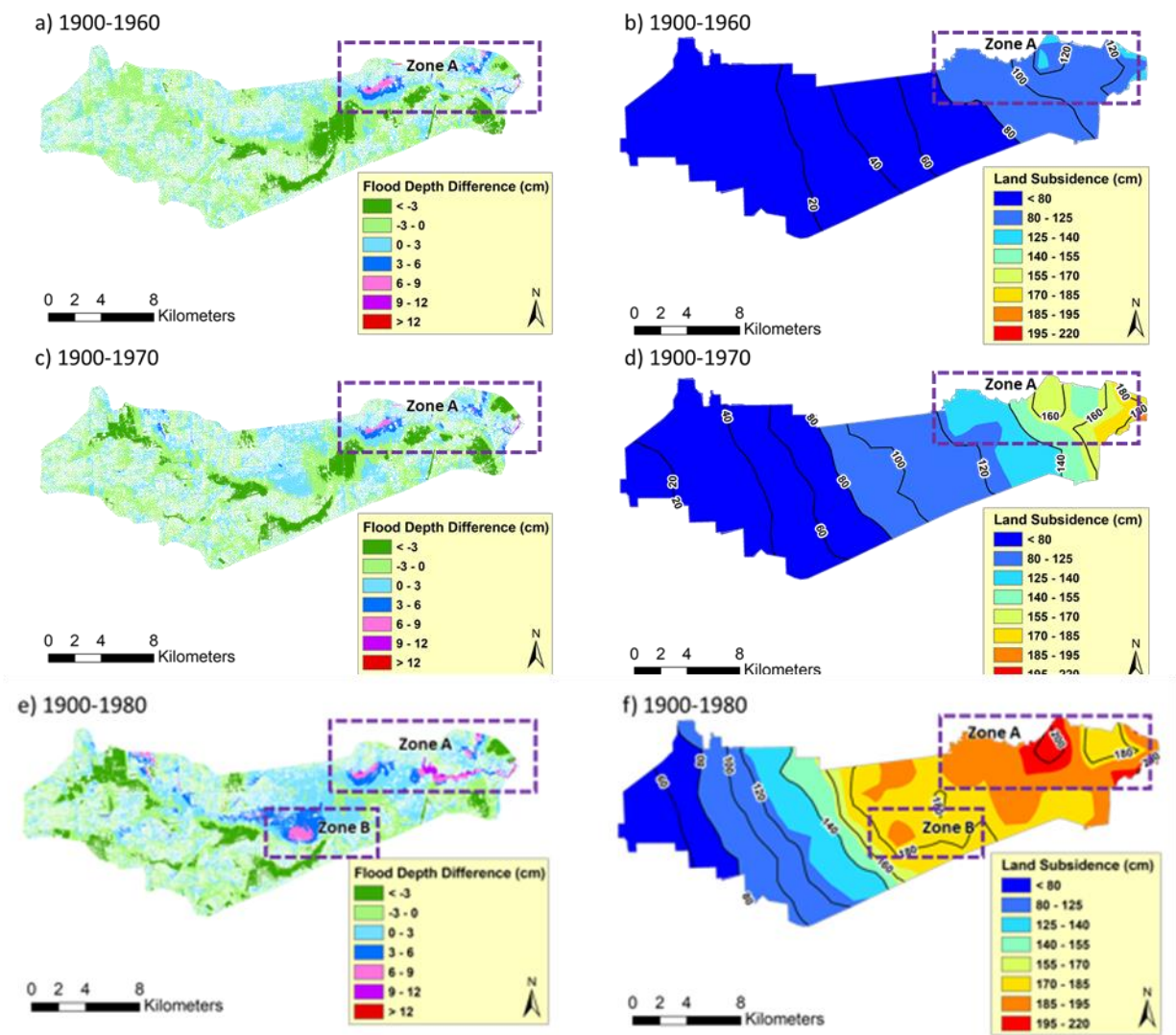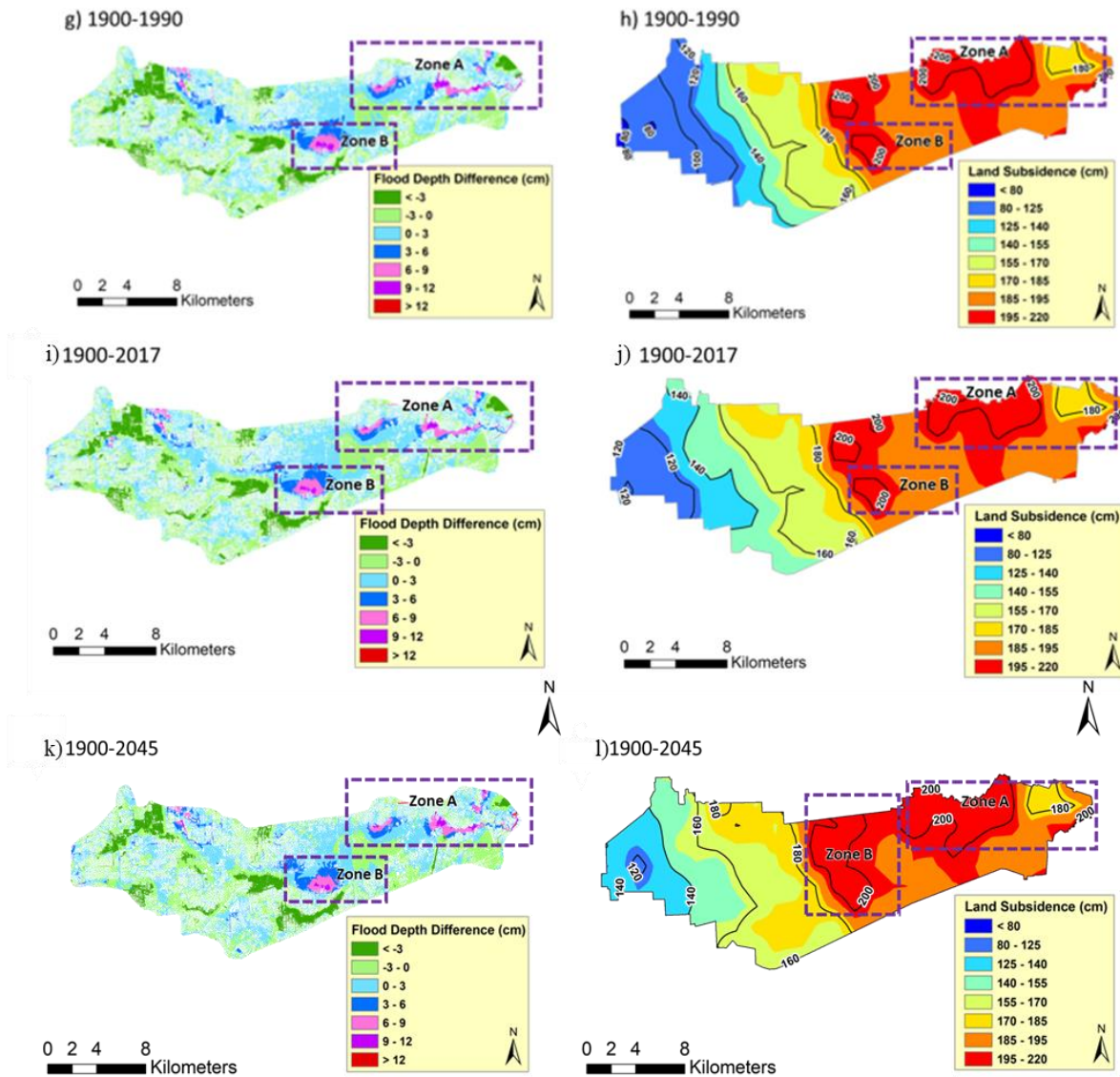
Figure 14: (a) Flood depth difference (FDD) between 1900 and 1960, (b) Land subsidence contours in the period of 1900 to 1960, (c) FDD between 1900 and 1970, (d) Land subsidence contours in the period of 1900 to 1970, (e) FDD between 1900 and 1980, (f) Land subsidence contours in the period of 1900 to 1980, (g) FDD between 1900 and 1990, (h) Land subsidence contours in the period of 1900 to 1990, (i) FDD between 1900 and 2017, (j) Land subsidence contours in the period of 1900 to 2017, (k) FDD between 1900 and 2045, and (l) Land subsidence contours in the period of 1900 to 2045.

Besides assessing spatial changes in land subsidence and flood depth individually, an evaluation of the relationship between FDD and land subsidence from 1900 to 2017 is also conducted. **Fig. 15** illustrates the ratio of the flood depth difference (FDD) to land subsidence in the period 1900 to 2017 and the period 1900 to 2045. It can be found that the highest ratio of FDD over land subsidence is about 10 %, indicating that the flood impacts caused by land subsidence are relatively minor compared to the magnitude of land subsidence itself. For example, the maximum land subsidence can reach approximately 2-m, while the changes in flood depth are significantly less with 12 cm at the same location.
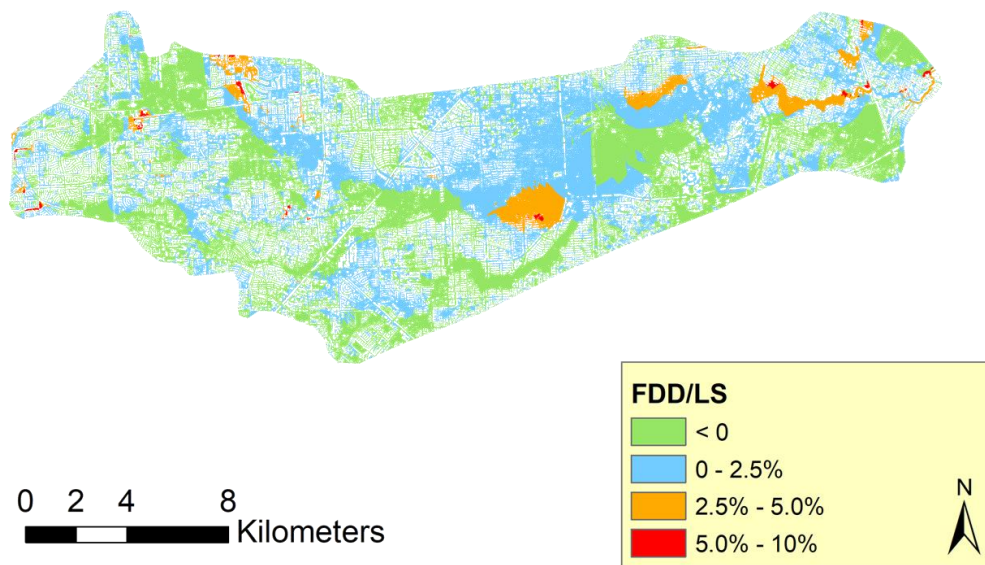
Figure 15: Ratio of the flood depth difference (FDD) to land subsidence in the period of (a) 1900 to 2017; (b) 1900 to 2045.

Table 5 quantifies and summarizes the area and percentage changes in FDD for different time periods, in which the negative value of FDD refers to a decrease in maximum flood depth compared to the year 1900. The results demonstrate that land subsidence may bring beneficial impacts with negative FDD for at least 48 % of the total inundated area of all six scenarios. In

1930 when land subsidence had just started, beneficial impacts could be found for 87 % of the total inundated area with negative FDD. The reason could be that minor land subsidence may help flood water drain faster downstream, resulting in shallower water depth for some places within the watershed. Areas with the increased FDD (0 to 9 cm) constitute only 13 % of the study domain in the period 1900 to 1930, then account for approximately 34 %, 37 %, 49 %, and 51 % in 1960, 1970, 1980, and 1990 respectively. It can be seen that major changes of FDD happened between 1970 and 1980 (37 % to 49 %), which corresponds to the same period with the largest land subsidence rate (**Fig. 5d**). The areas with relatively large flood depth difference (>9 cm) make up the rest 1 % at most in the period of 1900 to 1990.

Table 5: Changes of flood depth difference (cm) in the area (km^2) and percentage (%) of the simulation domain for various time periods (Pct means Percentage)

Flood Depth Difference (cm)	1900 - 1930		1900 - 1960		1900 - 1970		1900 - 1980		1900 - 1990		1900 - 2017	
	Area (km^2)	Percentage (%)	Area (km^2)	Percentage (%)	Area (km^2)	Percentage (%)	Area (km^2)	Percentage (%)	Area (km^2)	Percentage (%)	Area (km^2)	Percentage (%)
< -3.0	0.09	0.05	23.04	12.55	27.96	15.25	26.85	14.68	22.37	12.21	20.80	11.35
-3.0 – 0.0	160.82	86.84	98.17	53.47	86.86	47.37	65.67	35.91	65.34	35.66	68.22	37.23
0.0 – 3.0	24.17	13.05	56.89	30.99	63.49	34.62	70.90	38.77	74.75	40.80	75.98	41.46
3.1 – 6.0	0.07	0.04	3.82	2.08	4.01	2.19	13.40	7.33	13.39	7.31	11.33	6.18
6.1 – 9.0	0.02	0.01	1.46	0.80	0.94	0.51	4.82	2.64	5.59	3.05	5.77	3.15
9.1 – 12.0	0.01	0.01	0.15	0.08	0.07	0.04	1.15	0.63	1.71	0.93	1.07	0.58
> 12.0	0.02	0.00	0.07	0.03	0.03	0.02	0.07	0.04	0.07	0.04	0.09	0.05

Fit statistics and RMSD of flood depth for various scenarios using the 1900 condition as baseline are determined and presented in **Fig. 16a** and **b**, respectively. The Fit value indicates how similar two inundation areas are. **Fig. 16a** shows that the land subsidence does have an

influence on the extent of the inundated area, yet the changes appear to be limited since the values are always above 0.97. RMSD measures the difference in flood depth on a cell-by-cell basis between simulated results and reference. **Fig. 16b** shows that compared to the 1900 condition, flood depth increases starting from 1930 and reaches its climax in 1980, followed by a plateau and then decreases in 2045. These two indices (Fit and RMSD) demonstrate a similar trend in terms of inundation extent and flood depth, and the rapid changes in Fit and RMSD values between 1970 and 1980 coincide with the fast rate of land subsidence of the same time period as illustrated in **Fig. 16d**.
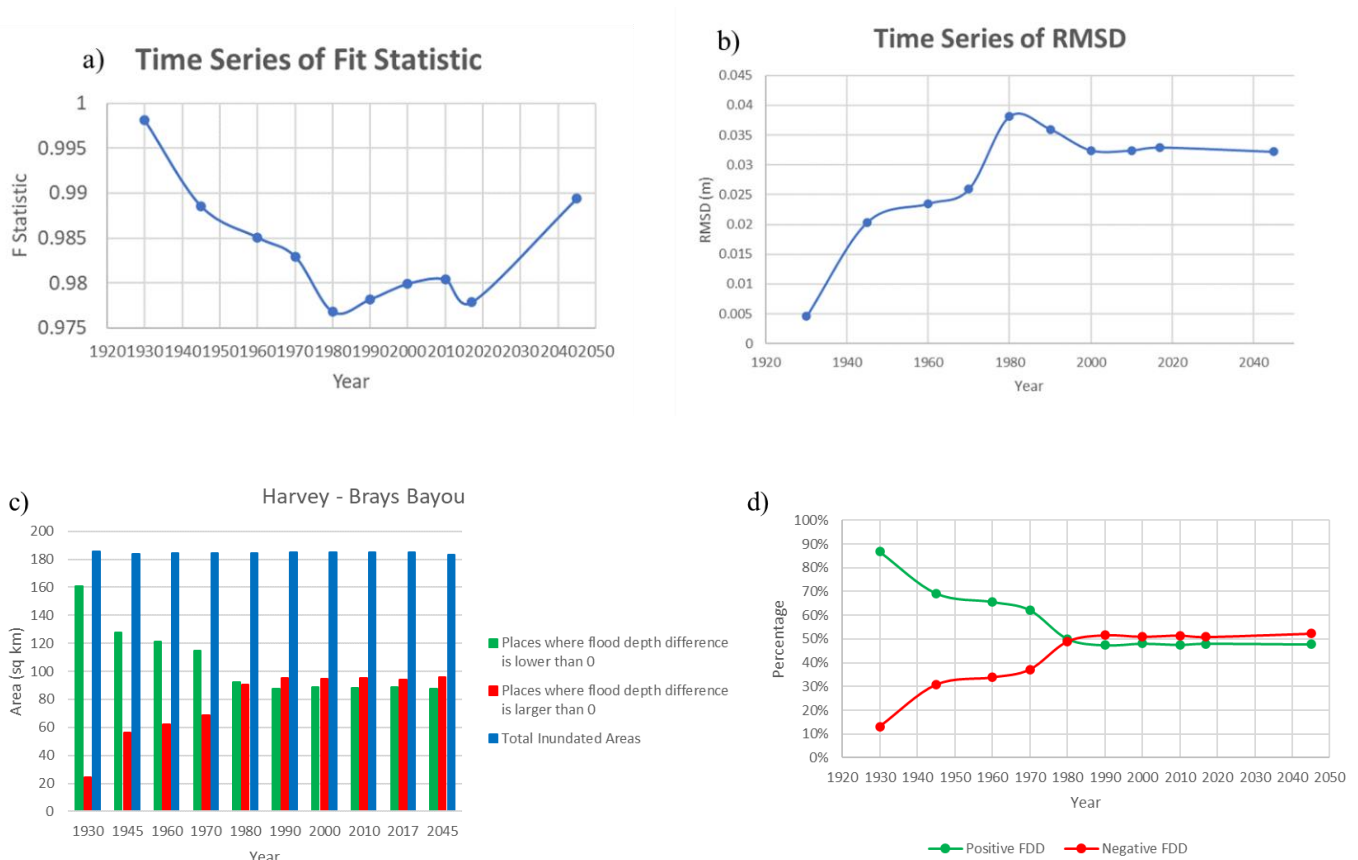
Figure 16: (a) Trend of the Fit Statistics of inundation area, (b) Trend of the flood depth RMSD, (c) Bar chart of inundation area changes, and (d) Trends of percentages of positive and negative flood depth difference (FDD)

Fig. 16c presents the temporal changes of the area in terms of flood depth difference (FDD). The blue bars represent the total inundated areas, and no significant changes are found over the years, indicating the impact of land subsidence on flood extent is minor in this study. The green and red bars represent the area of grids where the FDD is negative and positive, respectively. The area with positive and negative FDD show opposite trends over the years: the area with negative/positive FDD (green/red bars) tends to decrease/increase rapidly before 1980 and become stable after 1980. Areas with negative FDD (green) represent places that gain benefits from the land subsidence compared to the baseline condition (1900), and the benefit diminishes as land subsidence gets worse. To better quantify the relative area changes in FDD, the authors further calculate percentages of positive and negative FDD as shown in **Fig. 16d**. Both percentages of positive and negative FDD show steeper slopes during 1970 to 1980 than any other decades, which displays an agreement with the previous results of having the largest land subsidence rate between the same period (**Fig. 5d**). After 1980, these two percentages begin to stabilize due to the deceleration in land subsidence. Overall, the results imply that land subsidence has little impact on causing the change of flood inundation areas but does have an impact on the change of flood depth.

4.2   Sectional analyses of flood inundation

To further evaluate the spatial and temporal patterns of flood inundation at a local scale, the authors divide the Brays Bayou watershed into three sections: upstream (123.7 km^2) from its headwater to S. Gessner Rd., midstream (97.3 km^2) from S. Gessner Rd. to Main St., and downstream (56.9 km^2) of Main St. (**Fig. 17a**) (Bedient et al., 2002). **Fig. 17b** shows the temporal changes in median values of FDD for the upstream, midstream, and downstream sections. It can be found that median values show a decreasing trend from 1930 to 1945 in all three sections with negative FDD, indicating that flood water in these years is shallower than that

in 1900 condition. Median values of FDD at the downstream section start to increase since 1945 and become stable after 1980. Median values of FDD in the midstream section are observed to increase from 1960 and reach to their highest in 1980. Overall, median values of the upstream, midstream, and downstream sections show similar trends among years (first decrease and then increase) while the time of turning points varies. This may be associated with the non-uniform changes of land subsidence in various locations. As shown in **Table 6**, the midstream section features the highest annual subsidence rate during 1970 to 1980, consequently the median value of FDD in midstream shows the largest increase (from −0.26 cm to 0.45 cm) than those in the other two sections. After 1990, median values of FDD in all sections show minor changes, corresponding to the decreasing land subsidence rate at the same time (**Table 6**).
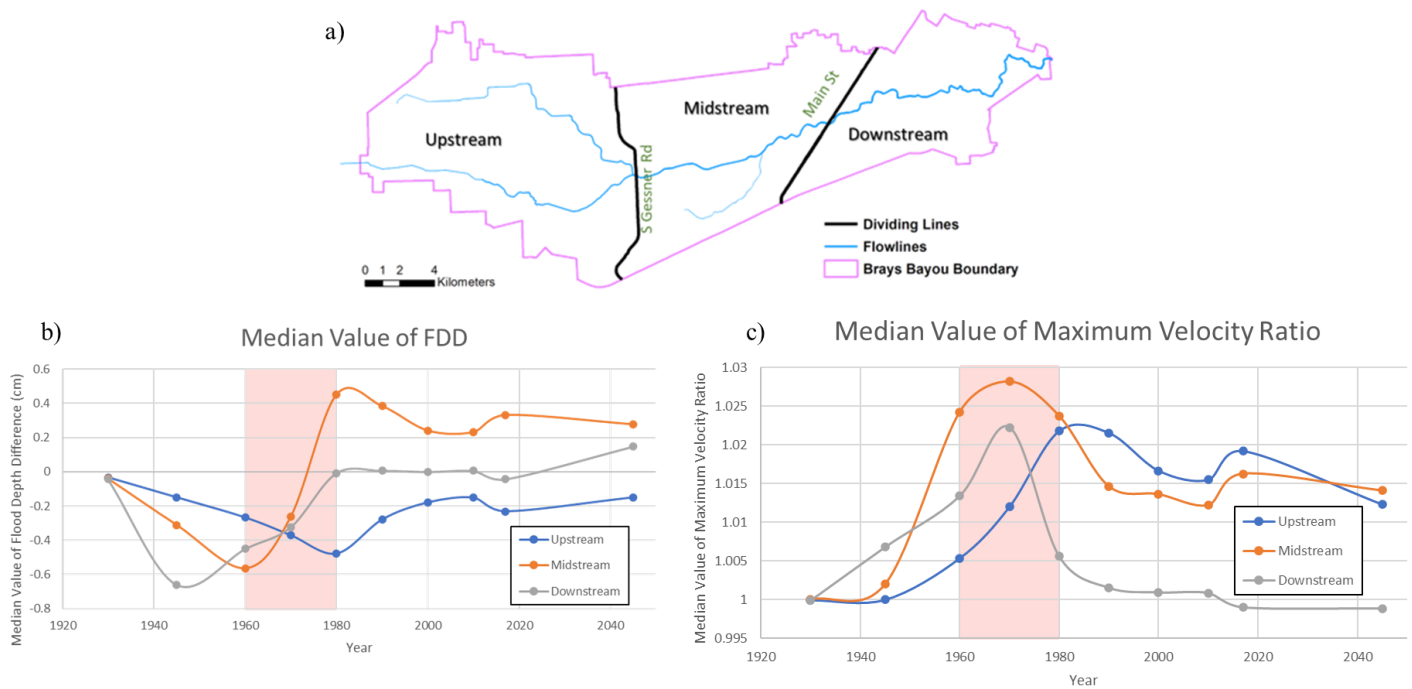
Figure 17: (a) Example map of dividing the Brays Bayou watershed into three sections; (b) Median values of the flood depth difference (FDD), and (c) median values of the flood velocity ratio (FVR) for upstream, midstream, and downstream sections.

Table 6: Average annual land subsidence rate (mm/yr) for up-, mid-, and downstream sections in Brays Bayou during different time periods.

Time Range	Upstream	Midstream	Downstream
1900-1930	0.0114	0.0133	0.0153
1930-1960	3.0435	17.2324	33.1066
1960-1970	28.6643	43.9189	44.7039
1970-1980	54.8193	73.9991	42.3358
1980-1990	36.0366	18.8718	6.1340
1990-2017	5.0227	0.0275	-0.1547

With the difference of the maximum flood depth within S1 simulations are assessed (**Figure 13** and **Figure 14**), comparison between S1, S2 and S3 results is conducted to evaluate the individual and compound effect of land subsidence and LULC. First, the ratio of the mean of the maximum flood depth in the corresponding year simulations to the baseline 2017 scenario (S1-7) are calculated and illustrated in **Figure 18** and **Figure 19**. It can be seen that the flood depth has been increased over time due to the growth in the land subsidence and urbanization in all scenarios. Besides, the impact of the change of land subsidence seems to be very minimal. Meanwhile the ratio in S2 increased from 0.499 to 1.076 from 1945 and 2045, suggesting that urbanization has larger impact on flood depth. In S3, the ratio increased from 0.499 to 1.009 from 1945 and 2045, which indicates that the combined effect of land subsidence and LULC may have helped with decreasing flood depth in 2045 compared with S1 and S1.
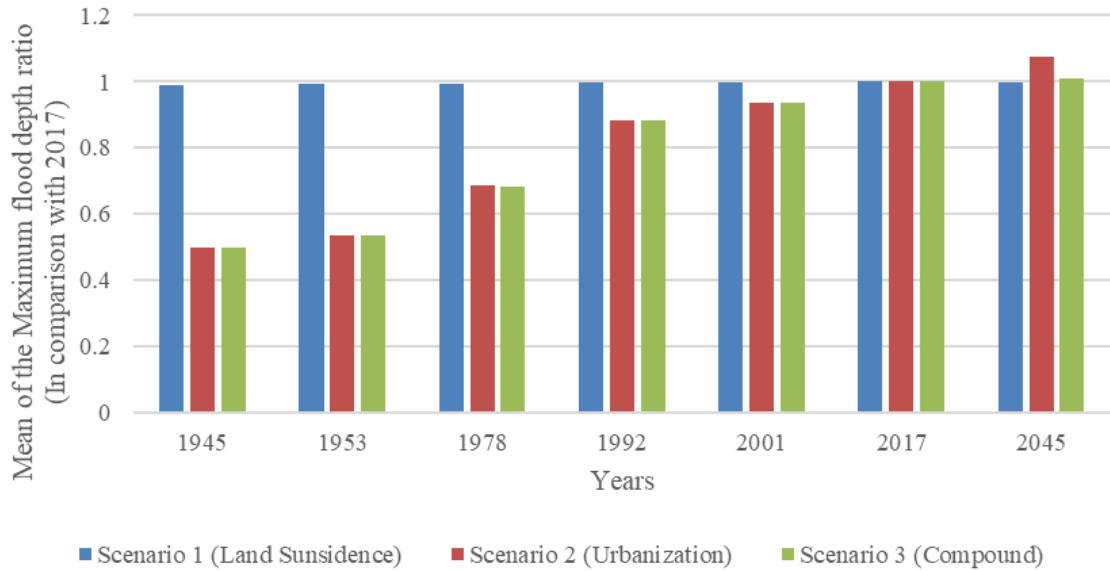
Figure 18: Bar chart of the ratio of the mean of maximum flood depth of three scenarios in different years.
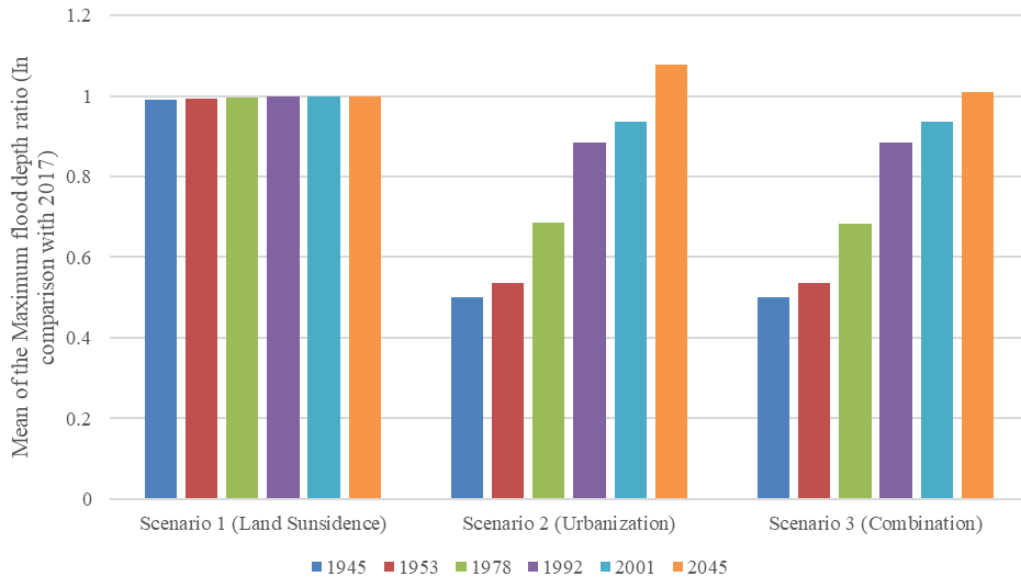
Figure 19: Bar chart of the ratio of the mean of maximum flood depth in different scenarios.

Chapter 5: Discussions

The results of this study indicate that land subsidence in general has a relatively minor influence on flood inundation compared to the magnitude of land subsidence itself. As shown in **Fig. 16**, the ratio of positive FDD values to corresponding land subsidence is mostly from 0 to 5 %, with the highest being about 10 %, This finding is similar with Yin et al. (2016), where their results show that the change in inundation depth is about 10 % of the magnitude of land subsidence. Also, it's found that flood water is deepened in places featuring evident land subsidence at a local scale. As illustrated in **Fig. 13 and 14**, changes of flood depth in Zone A and Zone B are higher than in the surrounding areas. Similar findings are also reported by Hsu et al. (2010) and Ito et al. (2015). Hsu et al. (2010) found that areas with serious land subsidence have increased inundation depth based on hydrodynamic modeling with hypothetical design flow rates. Ito et al. (2015) analyzed three flood events (occurred in 1970, 2004, and 2013) and concluded that water tends to accumulate in the area surrounded by slightly highlands (relative elevation +1–2 m).

In the analyses, some unique characteristics in the flood inundation are revealed due to the spatial heterogeneity and decadal evolution of land subsidence, which would otherwise be prohibited using traditional methods (e.g., surveyed DEM, field measurements/monitoring, remote sensing) to represent land subsidence. First, the effects of land subsidence are not only heterogeneous but even mixed with coexisting positive and negative impacts on flood inundation (**Figs. 14**, **Fig. 16c** and **16d**). The spatial heterogeneity is also reported by Yin et al. (2016), where they found land subsidence may have a non-linear impact on flooding. This is mainly due to the non-uniform rates of land subsidence between different time periods (Fig. S4). In 1930, approximately 88 % of inundated area features negative FDD compared to 1900 baseline condition (**Fig. 16c**), indicating most places actually gain benefits from land subsidence. As

illustrated in **Fig. 16d**, these benefits (green line) decline as land subsidence continues increasing until 1980. Percentages of negative (green line) and positive (red line) FDD intersect 1980, which marks a turning point when adverse impacts on flood depth caused by land subsidence outweigh the benefits in the study region. After 1980, land subsidence slows down and tends to cease, causing the areas with positive and negative impacts to stabilize till the present.

Second, the decadal evolution of land subsidence exerts cumulative effects on flood inundation, where previous land subsidence hotspots could be altered by later continuing land subsidence, i.e., emergence of new land subsidence hotspots in the watershed. As shown in **Fig. 5**, we can find that land subsidence hotspots have been drifting from downstream towards upstream over time, causing previously impacted areas to 'recover and even benefit'. From analyses of three sections (up-, mid-, and downstream) in Brays Bayou, flooding condition in midstream are the worst after 1970, where the median value of FDD is higher compared to the up- and downstream sections (**Fig. 16b**). The reason is that when the new land subsidence hotspot appeared midstream, flood water generated from upstream would accumulate and be held locally before flowing downstream. Unique from any other previous studies, the sectional evaluation reveals the locally deepened flood inundation and accelerated flood waves near the main channel, which could be overlooked if only the net impact (aggregated over the watershed) were considered.

Finally, the way land subsidence affects flood inundation in this study sharply contrasts how coastal inundation is exacerbated by land subsidence (e.g., Shirzaei and Bürgmann, 2018; Catalao et al., 2020). For instance, the future 100-yr inundation maps estimated by Shirzaei and Bürgmann (2018) showed that land subsidence would amplify flood risk up to 90 % compared with scenarios only considering the sea level rise. Catalato et al. (2020) compared DEM with the sum of tide height, sea level rise, and cumulative land subsidence and estimated 25 % increase in

flood area for future scenarios. In contrast, flood inundation areas simulated in this study for different years do not show significant changes due to land subsidence (blue bars in **Fig. 16c**), while areas with positive and negative FDD internally vary throughout years. The reason is that flood inundation is dynamic due to the movement of flood wave, while coastal inundation is static and controlled by the elevation difference between land and sea. This explains our findings where certain levels of land subsidence could reduce overland flood depth by accelerating flood velocity, whereas worse coastal inundation is almost definite given land subsidence (Wang et al., 2012; Yin et al., 2013; Shirzaei and Bürgmann, 2018; Catalao et al., 2020).

This study demonstrates the capability of HEC-RAS 2D for modeling the changes of flood inundation caused by land subsidence. However, due to some limitations related to the model itself (HEC-RAS version 5.0), the uniform rainfall is applied, and infiltration is neglected by our simulation, as explained before in detail in the data section. These limitations/assumptions, though acceptable in this study, might be problematic for a different study region or storm events. As a remedy, newer versions of HEC-RAS will allow spatially varied precipitation as input as well as more realistic representation of the infiltration process, which is promising for broadening the applicability of our approaches (Brunner, 2021). Additionally, previous studies have reported sea level rise exacerbates coastal flooding, as another major contributor (besides land subsidence) to the total relative elevation difference between land and sea (Wang et al., 2012; Dang et al., 2018; Zeiger and Hubbart, 2021; Zhao et al., 2021; El Shinawi, 2022). Therefore, one clear future direction is to incorporate sea level rise into the analysis framework of this study. It's expected that storm surge, as another hazard from tropical cyclones, will be aggravated by sea level rise and jointly impact a coastal region along with the rainfall-induced inland flooding.

Chapter 6: Conclusion and Future Research

This chapter presents a summary of the findings and conclusions from previous chapters and provides suggestions for future research.

CONCLUSIONS

This doctoral study provides fresh insights on the impact from land subsidence on flood inundation, which is uniquely enabled by a retrospective, 145-year, physics-based modeling by Liu et al. (2020) considering groundwater withdrawal and the consequent aquifer-system compaction. Hydrodynamic simulation of flood inundation from Hurricane Harvey over the topologies in different historical times from 1900 to 2045 depicts realistic pictures of how Harvey flood could have evolved over the 145 years due to continuous land subsidence in Brays Bayou, Texas. This research is among the first to shed light on the consequence of land subsidence on flooding that is continuous both in space and time.

Specifically, the results show that the overall change of flood depth caused by land subsidence is relatively minor compared to the magnitude of land subsidence itself. The results also demonstrate that the impact from changes of urbanization is larger than that from land subsidence. Over the course of 145 years, the worst impacted location in Brays Bayou experiences only 12 cm deepened flood water due to approximately 2-m subsidence at the same location. However, the impact from land subsidence on flood depth is non-linear in time, where effects from previous land subsidence hotspots could be altered by later continuing land subsidence, i.e., emergence of new land subsidence hotspots in the watershed. Specifically in Brays Bayou, later-occurring subsidence in upstream counteracts the preceding downstream subsidence, mitigating previously increased flood depth. Spatially, change in flood depth due to

47

the land subsidence is not only heterogeneous but also mixed with coexisting deeper and shallower flood water. Land subsidence could reduce flood depth but accelerate flood velocity locally, while causing flood water to pond in other locations, e.g., lower main stem with mild slope.

The results and analysis of this research demonstrate the change of flood characteristics caused by land subsidence and LULC and advance the knowledge of how it changes hydrodynamic features. The research evaluates the individual and combined effects of land subsidence and land cover at Brays Bayou watershed by setting up three different scenarios. The output from the models is analyzed as a whole watershed and also in three divided sections in order to evaluate the hydrological responses. Since most previous studies focused on the analysis with individual factors, the results of this study provide critical information for understanding flood characteristics by relating the hydrological responses to their characteristics. The hydrodynamic simulation reveals the impacts from land subsidence and LULC regarding flood depth, inundation extent, and flow velocity; The effects of land subsidence and LULC on flooding are not only heterogeneous but even mixed with both positive and negative impact.

The findings of this study highlight the need for a comprehensive assessment of human activities in the study area and the adaptation of sustainable LULC practices, such as close supervision of bare land restoration and bush land conservation, making grazing lands available through the restoration of degraded and impoverished lands, and limiting further expansion of cultivated areas. Therefore, sustainable land use planning and management, appropriate implementation of forest, soil, and water conservation measures, and provision of alternative livelihood strategies should be implemented for local communities in the study area in order to reverse unfavorable situations associated with LULC changes.

This research has an influence on communities in urban planning, watershed

management, and flood control and provides valuable insight for stakeholders of sustainable development policies and practices (short- and long-term). Flexible and adaptable research methodologies can be used in other watersheds in various regions both domestically and abroad.

FUTURE RESEARCH

It is important to acknowledge that there are additional aspects that can be taken into account while conducting simulations. The assessment in this study is done with a state-of-the-art, thoroughly validated hydrodynamic model, however, it possesses some limitations that attention has been concentrated on Brays Bayou watershed in Harris County, with no attention given to the impact of the surrounding regions which has the most severe land subsidence from 1900 to 2045, which make the results and findings site specific. Furthermore, the hydraulic model itself can be further improved by using less computation time, using data with finer resolution and adding 1D structures like road, railway embankment, etc. Storm events with other amount of precipitation (real events and design events) can also be simulated in future studies. Lastly, this study only considered different land cover in the model without taking the compaction of the soils during urbanization development, which could also have a possible influence on flood inundation aspects.

The doctoral research includes studies to examine the H&H modeling as introduced in Chapter 2, 3 4 and 5. Future research should investigate the methods for automating the calibration of hydrologic/hydraulic models for more applications in rapid hazard response and mitigation. For the research on watershed response, incorporating sea level rise, storm surge or other climate change factor into this study's framework is one of the future directions and incorporating aspects like soil compaction to infiltration using other storm events in the model in a larger scale study area like other large watersheds, Harris County or other regions being

another direction.

ACKNOWLEDGMENT

References

Abidin, H. Z., Andreas, H., Gumilar, I., & Wibowo, I. R. R. (2015). On correlation between urban development, land subsidence and flooding phenomena in Jakarta. Proceedings of the International Association of Hydrological Sciences, 370, 15-20.

Ahmadlou, M., Al-Fugara, A. K., Al-Shabeeb, A. R., Arora, A., Al-Adamat, R., Pham, Q. B., ... & Sajedi, H. (2021). Flood susceptibility mapping and assessment using a novel deep learning model combining multilayer perceptron and autoencoder neural networks. Journal of Flood Risk Management, 14(1), e12683.

Bass, B., Juan, A., Gori, A., Fang, Z., & Bedient, P. (2017). 2015 Memorial Day flood impacts for changing watershed conditions in Houston. Natural Hazards Review, 18(3), 05016007.

Bates, P. D., & De Roo, A. P. J. (2000). A simple raster-based model for flood inundation simulation. Journal of hydrology, 236(1-2), 54-77.

Bedient, P. B., Holder, A., & Vieux, B. E. (2002). A radar-based flood alert system (FAS) designed for Houston, Texas. In Global Solutions for Urban Drainage (pp. 1-10).

Bedient, P. B., Holder, A., Benavides, J. A., & Vieux, B. E. (2003). Radar-based flood warning system applied to Tropical Storm Allison. Journal of Hydrologic Engineering, 8(6), 308-318.

Brunner, G. W. (2016a). HEC-RAS River Analysis System, 2D modeling user's manual version 5.0. Davis: US Army Corps of Engineers, hydrologic engineering center.

Brunner, G. W. (2016b). HEC-RAS River Analysis System hydraulic reference manual, Ver. 5.0. Davis, CA, USA: US Army Corps of Engineers, Hydrologic Engineering Center, cpd-69.

Carisi, F., Domeneghetti, A., Gaeta, M. G., & Castellarin, A. (2017). Is anthropogenic land subsidence a possible driver of riverine flood-hazard dynamics? A case study in Ravenna, Italy. Hydrological Sciences Journal, 62(15), 2440-2455.

Catalao, J., Raju, D., & Nico, G. (2020). InSAR maps of land subsidence and sea level scenarios to quantify the flood inundation risk in coastal cities: The case of Singapore. Remote Sensing, 12(2), 296.

Chan, F. K. S., Mitchell, G., Adekola, O., & McDonald, A. (2012). Flood risk in Asia's urban mega-deltas: Drivers, impacts and response. Environment and Urbanization ASIA, 3(1), 41-61.

Chow, V. (1959). T. 1959 Open-Channel Hydraulics. MCGraw Hiu.

Chun, B., Hur, M., & Won, J. (2021). Impacts of Thermal Environments on Health Risk: A Case Study of Harris County, Texas. International Journal of Environmental Research and Public Health, 18(11), 5531.

Costabile, P., Costanzo, C., Ferraro, D., Macchione, F., & Petaccia, G. (2020). Performances of the new HEC-RAS version 5 for 2-D hydrodynamic-based rainfall-runoff simulations at basin scale: Comparison with a state-of-the art model. Water, 12(9), 2326.

Costabile, P., Costanzo, C., Ferraro, D., Macchione, F., & Petaccia, G. (2020). Performances of the new HEC-RAS version 5 for 2-D hydrodynamic-based rainfall-runoff simulations at basin scale: Comparison with a state-of-the art model. Water, 12(9), 2326.

Dang, T. D., Cochrane, T. A., & Arias, M. E. (2018). Future hydrological alterations in the Mekong Delta under the impact of water resources development, land subsidence and sea level rise. Journal of Hydrology: Regional Studies, 15, 119-133.

Das, S. (2019). Geospatial mapping of flood susceptibility and hydro-geomorphic response to the floods in Ulhas basin, India. Remote Sensing Applications: Society and Environment, 14, 60-74.

David, A., & Schmalz, B. (2020). Flood hazard analysis in small catchments: Comparison of hydrological and hydrodynamic approaches by the use of direct rainfall. Journal of Flood Risk Management, 13(4), e12639.

Dixon, T. H., Amelung, F., Ferretti, A., Novali, F., Rocca, F., Dokka, R., ... & Whitman, D.

(2006). Subsidence and flooding in New Orleans. Nature, 441(7093), 587-588.

Edwards, D. (2021). Flood Inundation Mapping for Lower Region of Neches River Watershed Using One–Dimensional and Two–Dimensional HEC-RAS Modeling (Doctoral dissertation, Lamar University-Beaumont).

Emanuel, K. (2017). Assessing the present and future probability of Hurricane Harvey's rainfall. Proceedings of the National Academy of Sciences, 114(48), 12681-12684.

EM-DAT. Disaster Profiles, (2020). The OFDA/CRED International Disaster Database, Dec 2020. Retrieved from https://public.emdat.be/Farooq, M., Shafique, M., & Khattak, M. S. (2019). Flood hazard assessment and mapping of River Swat using HEC-RAS 2D model and high-resolution 12-m TanDEM-X DEM (WorldDEM). Natural Hazards, 97(2), 477-492.

FEMA. (2020). FIMA NFIP Redacted Claims Data Set, Dec 2020. Retrieved from https://www.fema.gov/openfema-data-page/fima-nfip-redacted-claims

Galloway, D. L., Jones, D. R., & Ingebritsen, S. E. (Eds.). (1999). Land subsidence in the United States (Vol. 1182). US Geological Survey.

Gambolati, G., & Teatini, P. (2015). Geomechanics of subsurface water withdrawal and injection. Water Resources Research, 51(6), 3922-3955.

Gao, S., Zhang, J., Li, D., Jiang, H., & Fang, Z. N. (2020). Evaluation of Multiradar Multisensor and Stage IV Quantitative Precipitation Estimates during Hurricane Harvey. Natural Hazards Review, 22(1), 04020057.

Garcia, M., Juan, A., & Bedient, P. (2020). Integrating Reservoir Operations and Flood Modeling with HEC-RAS 2D. Water, 12(8), 2259.

Goodell, C. (2014, December 8). Including Channel Bathymetry into your Terrain. The RAS Solution. https://www.kleinschmidtgroup.com/ras-post/including-channel-bathymetry-into-your-terrain/

Golian, M., Saffarzadeh, A., Katibeh, H., Mahdad, M., Saadat, H., Khazaei, M., ... & Dashti Barmaki, M. (2021). Consequences of groundwater overexploitation on land subsidence in Fars Province of Iran and its mitigation management programme. Water and Environment Journal, 35(3), 975-985.

Grimaldi, S., Schumann, G. P., Shokri, A., Walker, J. P., & Pauwels, V. R. N. (2019). Challenges, opportunities, and pitfalls for global coupled hydrologic-hydraulic modeling of floods. Water Resources Research, 55(7), 5277-5300.

Gupta, H. V., Kling, H., Yilmaz, K. K., & Martinez, G. F. (2009). Decomposition of the mean squared error and NSE performance criteria: Implications for improving hydrological modelling. Journal of hydrology, 377(1-2), 80-91.

Habib, E., Larson, B. F., & Graschel, J. (2009). Validation of NEXRAD multisensor precipitation estimates using an experimental dense rain gauge network in south Louisiana. Journal of Hydrology, 373(3-4), 463-478.

Handbook of Texas Online, "WILLOW WATERHOLE BAYOU," accessed August 11, 2020, http://www.tshaonline.org/handbook/online/articles/rhw07.

Hanson, S., Nicholls, R., Ranger, N., Hallegatte, S., Corfee-Morlot, J., Herweijer, C., & Chateau, J. (2011). A global ranking of port cities with high exposure to climate extremes. Climatic change, 104(1), 89-111.

HCFCD, Harris County Flood Control District. (2020a). Model and Map Management (M3) System, accessed in 2020. Retrieved from https://www.hcfcd.org/Interactive-Mapping-Tools/MODEL-AND-MAP-MANAGEMENT-M3-SYSTEM

HCFCD, Harris County Flood Control District. (2020b). Harris County Flood Warning System, accessed in 2020. https://www.harriscountyfws.org/?View=full

HCFCD, Harris County Flood Control District. (2020c). Historical High Water Marks, accessed

in 2020. Available at https://www.arcgis.com/home/item.html?id=bd266d344dab42b993c5d4f0b4599282HCFCD, Harris County Flood Control District. (2020d). Two-Dimensional Modeling Guidelines, accessed in 2018. Available at https://www.bidnet.com/bneattachments?/528797891.pdf

Highfield, W. E., Brody, S. D., Atoba, K., & Blessing, R. (2017). Identifying the future costs of flooding in the Houston-Galveston region. Center for Texas Beaches and Shores. Texas A&M University, Galveston Campus.

Hinkel, J., Lincke, D., Vafeidis, A. T., Perrette, M., Nicholls, R. J., Tol, R. S., ... & Levermann, A. (2014). Coastal flood damage and adaptation costs under 21st century sea-level rise. Proceedings of the National Academy of Sciences, 111(9), 3292-3297.

Hoffmann, J., Leake, S. A., Galloway, D. L., & Wilson, A. M. (2003). MODFLOW-2000 groundwater model--User guide to the subsidence and aquifer-system compaction (SUB) package. Geological Survey Washington DC.

Holzer, T. L., & Bluntzer, R. L. (1984). Land Subsidence Near Oil and Gas Fields, Houston, Texas a. Groundwater, 22(4), 450-459.

Holzer, T. L., & Johnson, A. I. (1985). Land subsidence caused by ground water withdrawal in urban areas. GeoJournal, 11(3), 245-255.

Hsiao, S. C., Fu, H. S., Chen, W. B., Chang, T. Y., Wu, H. L., & Liang, T. Y. (2022). Assessment of future possible maximum flooding extent in the midwestern coastal region of Taiwan resulting from sea-level rise and land subsidence. Environmental Research Communications, 4(9), 095007.

Hsu, P. H., Su, W. R., & Tsai, C. H. (2010, July). Land subsidence analysis and inundation prediction based on multi-temporal digital elevation model data. In 2010 IEEE International Geoscience and Remote Sensing Symposium (pp. 3339-3342). IEEE.

Hussein, K., Alkaabi, K., Ghebreyesus, D., Liaqat, M. U., & Sharif, H. O. (2020). Land use/land cover change along the Eastern Coast of the UAE and its impact on flooding risk. Geomatics, Natural Hazards and Risk, 11(1), 112-130.

Ito, Y., Chen, H., Sawamukai, M., Su, T., & Tokunaga, T. (2015). An analysis on the relationship between land subsidence and floods at the Kujukuri Plain in Chiba Prefecture, Japan. Proceedings of the International Association of Hydrological Sciences, 372, 163-167.

Jiang, H., Zhang, J., Liu, Y., Li, J., & Fang, Z. N. (2023). Does flooding get worse with subsiding land? Investigating the impacts of land subsidence on flood inundation from Hurricane Harvey. Science of the total environment, 865, 161072.

Jonkman, S. N., Godfroy, M., Sebastian, A., & Kolen, B. (2018). Brief communication: Loss of life due to Hurricane Harvey. Natural Hazards and Earth System Sciences, 18(4), 1073-1078.

Karim, I. R., Hassan, Z. F., Abdullah, H. H., & Alwan, I. A. (2021). 2D-HEC-RAS Modeling of Flood Wave Propagation in a Semi-Arid Area Due to Dam Overtopping Failure. Civil Engineering Journal, 7(9), 1501-1514.

Kasmarek, M.C. (2013). Hydrogeology and Simulation of Groundwater Flow and Land-Surface Subsidence in the Northern Part of the Gulf Coast Aquifer System, Texas, 1891–2009, U.S. Geological Survey Scientific Investigations Report 2012–5154.

Kasmarek, M. C., Gabrysch, R. K., & Johnson, M. R. (2009). Estimated land-surface subsidence in Harris County, Texas, 1915-17 to 2001. US Department of the Interior, US Geological Survey.

Kellens, W., Terpstra, T., & De Maeyer, P. (2013). Perception and communication of flood risks: A systematic review of empirical research. Risk Analysis: An International Journal, 33(1), 24-49.

Khan, S. I., Hong, Y., Wang, J., Yilmaz, K. K., Gourley, J. J., Adler, R. F., ... & Irwin, D. (2010). Satellite remote sensing and hydrologic modeling for flood inundation mapping in Lake Victoria basin: Implications for hydrologic prediction in ungauged basins. IEEE Transactions on

Geoscience and Remote Sensing, 49(1), 85-95.

KIM, V., TANTANEE, S., & SUPARTA, W. (2020). GIS-BASED FLOOD HAZARD MAPPING USING HEC-RAS MODEL: A CASE STUDY OF LOWER MEKONG RIVER, CAMBODIA. Geographia Technica, 15(1).

Knutson, T. R., McBride, J. L., Chan, J., Emanuel, K., Holland, G., Landsea, C., ... & Sugi, M. (2010). Tropical cyclones and climate change. Nature geoscience, 3(3), 157-163.

Kron, W. (2013). Coasts: the high-risk areas of the world. Natural hazards, 66(3), 1363-1382.

Legates, D. R., & McCabe Jr, G. J. (1999). Evaluating the use of "goodness-of-fit" measures in hydrologic and hydroclimatic model validation. Water resources research, 35(1), 233-241.

Li, X., Rankin, C., Gangrade, S., Zhao, G., Lander, K., Voisin, N., ... & Gao, H. (2021). Evaluating precipitation, streamflow, and inundation forecasting skills during extreme weather events: A case study for an urban watershed. Journal of Hydrology, 603, 127126.

Lin, Y., & Mitchell, K. E. (2005). 1.2 the NCEP stage II/IV hourly precipitation analyses: Development and applications. In Proceedings of the 19th Conference Hydrology, American Meteorological Society, San Diego, CA, USA (Vol. 10).

Liu, Y., Li, J., & Fang, Z. N. (2019). Groundwater level change management on control of land subsidence supported by borehole extensometer compaction measurements in the Houston-Galveston Region, Texas. Geosciences, 9(5), 223.

Liu, Y., Li, J., Fasullo, J., & Galloway, D. L. (2020). Land subsidence contributions to relative sea level rise at tide gauge Galveston Pier 21, Texas. Scientific reports, 10(1), 1-11.

Li, H., Zhu, L., Guo, G., Zhang, Y., Dai, Z., Li, X., ... & Teatini, P. (2021). Land subsidence due to groundwater pumping: hazard probability assessment through the combination of Bayesian model and fuzzy set theory. Natural Hazards and Earth System Sciences, 21(2), 823-835.

Li, X., Rankin, C., Gangrade, S., Zhao, G., Lander, K., Voisin, N., ... & Gao, H. (2021).

Evaluating precipitation, streamflow, and inundation forecasting skills during extreme weather events: A case study for an urban watershed. Journal of Hydrology, 603, 127126.

Li, J., & Bortolot, Z. J. (2022). Quantifying the impacts of land cover change on catchment-scale urban flooding by classifying aerial images. Journal of Cleaner Production, 344, 130992.

Marfai, M. A., & King, L. (2007). Monitoring land subsidence in Semarang, Indonesia. Environmental geology, 53, 651-659.

Mattocks, C., & Forbes, C. (2008). A real-time, event-triggered storm surge forecasting system for the state of North Carolina. Ocean Modelling, 25(3-4), 95-119.

Mediero, L., Garrote, L., & Martín-Carrasco, F. J. (2011). Probabilistic calibration of a distributed hydrological model for flood forecasting. Hydrological sciences journal, 56(7), 1129-1149.

Michel-Kerjan, E., & Kunreuther, H. (2011). Redesigning flood insurance. Science, 333(6041), 408-409.

Miller, R. L., Fram, M., Fujii, R., & Wheeler, G. (2008). Subsidence reversal in a re-established wetland in the Sacramento-San Joaquin Delta, California, USA. San Francisco Estuary and Watershed Science, 6(3).

Miller, M. M., & Shirzaei, M. (2019). Land subsidence in Houston correlated with flooding from Hurricane Harvey. Remote Sensing of Environment, 225, 368-378.

Modrick, T. M., & Georgakakos, K. P. (2015). The character and causes of flash flood occurrence changes in mountainous small basins of Southern California under projected climatic change. Journal of Hydrology: Regional Studies, 3, 312-336.

Moe, I. R., Kure, S., Januriyadi, N. F., Farid, M., Udo, K., Kazama, S., & Koshimura, S. (2017). Future projection of flood inundation considering land-use changes and land subsidence in Jakarta, Indonesia. Hydrological Research Letters, 11(2), 99-105.

Morrs, R.E., 2010. Interactions among flood predictions, decisions, and outcomes: synthesis of three cases. Nat. Hazards Rev. 11 (3), 83–96.

Morton, R. A., Bernier, J. C., & Barras, J. A. (2006). Evidence of regional subsidence and associated interior wetland loss induced by hydrocarbon production, Gulf Coast region, USA. Environmental Geology, 50(2), 261-274.

Munawar, H. S., Hammad, A., Ullah, F., & Ali, T. H. (2019, December). After the flood: A novel application of image processing and machine learning for post-flood disaster management. In Proceedings of the 2nd International Conference on Sustainable Development in Civil Engineering (ICSDC 2019), Jamshoro, Pakistan (pp. 5-7).

Musser, J. W., Watson, K. M., & Gotvald, A. J. (2017). Characterization of peak streamflows and flood inundation at selected areas in North Carolina following Hurricane Matthew, October 2016 (No. 2017-1047). US Geological Survey.

Navarro-Hernández, M., Valdés-Abellán, J., Tomás, R., Tessitore, S., Ezquerro, P., & Herrera, G. (2022). Flood inundation mapping using 2-d streamflow hydraulic modeling and land subsidence data from InSAR observations in the Alto Guadalentin valley, Spain (No. EGU22-3787). Copernicus Meetings.

Nelson, B. R., Prat, O. P., Seo, D. J., & Habib, E. (2016). Assessment and implications of NCEP Stage IV quantitative precipitation estimates for product intercomparisons. Weather and Forecasting, 31(2), 371-394.

NOAA (2020). Storm Events Database. Available at NOAA site: https://www.ncdc.noaa.gov/stormevents/

Noori, N., Kalin, L., Sen, S., Srivastava, P., & Lebleu, C. (2016). Identifying areas sensitive to land use/land cover change for downstream flooding in a coastal Alabama watershed. Regional environmental change, 16, 1833-1845.

Ongdas, N., Akiyanova, F., Karakulov, Y., Muratbayeva, A., & Zinabdin, N. (2020). Application of HEC-RAS (2D) for flood hazard maps generation for Yesil (Ishim) river in Kazakhstan. Water, 12(10), 2672.

Ouyang, M., Ito, Y., & Tokunaga, T. (2020). Local land subsidence exacerbates inundation hazard to the Kujukuri Plain, Japan. Proceedings of the International Association of Hydrological Sciences, 382, 657-661.

Pabi, O., Egyir, S., & Attua, E. M. (2021). Flood hazard response to scenarios of rainfall dynamics and land use and land cover change in an urbanized river basin in Accra, Ghana. City and Environment Interactions, 12, 100075.

Pacheco-Martínez, J., Hernandez-Marín, M., Burbey, T. J., González-Cervantes, N., Ortíz-Lozano, J. Á., Zermeño-De-Leon, M. E., & Solís-Pinto, A. (2013). Land subsidence and ground failure associated to groundwater exploitation in the Aguascalientes Valley, México. Engineering Geology, 164, 172-186.

Patel, D. P., Ramirez, J. A., Srivastava, P. K., Bray, M., & Han, D. (2017). Assessment of flood inundation mapping of Surat city by coupled 1D/2D hydrodynamic modeling: a case application of the new HEC-RAS 5. Natural Hazards, 89(1), 93-130.

Penning-Rowsell, E., Floyd, P., Ramsbottom, D., & Surendran, S. (2005). Estimating injury and loss of life in floods: a deterministic framework. Natural hazards, 36(1-2), 43-64.

Pérez-Falls, Z., Martínez-Flores, G., & Sarychikhina, O. (2022). Land Subsidence Detection in the Coastal Plain of Tabasco, Mexico Using Differential SAR Interferometry. Land, 11(9), 1473.

Phillips, J. V., & Tadayon, S. (2006). Selection of Manning's roughness coefficient for natural and constructed vegetated and non-vegetated channels, and vegetation maintenance plan guidelines for vegetated channels in Central Arizona. US Geological Survey.

Rajib, A., Liu, Z., Merwade, V., Tavakoly, A. A., & Follum, M. L. (2020). Towards a large-scale

locally relevant flood inundation modeling framework using SWAT and LISFLOOD-FP. Journal of Hydrology, 581, 124406.

Rodolfo, K. S., & Siringan, F. P. (2006). Global sea-level rise is recognized, but flooding from anthropogenic land subsidence is ignored around northern Manila Bay, Philippines. Disasters, 30(1), 118-139.

Schmidt, C. W. (2015). Delta subsidence: an imminent threat to coastal populations.

Stork. S.V. & Sneed M. (2002). Houston-Galveston Bay area, Texas, from Space—a new tool for mapping land subsidence. US Geological Survey Fact Sheet 110, 2.

Shirzaei, M., & Bürgmann, R. (2018). Global climate change and local land subsidence exacerbate inundation risk to the San Francisco Bay Area. Science advances, 4(3), eaap9234.

Shrestha, A., Bhattacharjee, L., Baral, S., Thakur, B., Joshi, N., Kalra, A., & Gupta, R. (2020, May). Understanding Suitability of MIKE 21 and HEC-RAS for 2D Floodplain Modeling. In World Environmental and Water Resources Congress 2020: Hydraulics, Waterways, and Water Distribution Systems Analysis (pp. 237-253). Reston, VA: American Society of Civil Engineers.

Shustikova, I., Domeneghetti, A., Neal, J. C., Bates, P., & Castellarin, A. (2019). Comparing 2D capabilities of HEC-RAS and LISFLOOD-FP on complex topography. Hydrological Sciences Journal, 64(14), 1769-1782.

Sun, H., Grandstaff, D., & Shagam, R. (1999). Land subsidence due to groundwater withdrawal: potential damage of subsidence and sea level rise in southern New Jersey, USA. Environmental Geology, 37, 290-296.

Tayefi, V., Lane, S. N., Hardy, R. J., & Yu, D. (2007). A comparison of one-and two-dimensional approaches to modelling flood inundation over complex upland floodplains. Hydrological Processes: An International Journal, 21(23), 3190-3202.

Teatini, P., Ferronato, M., Gambolati, G., Bertoni, W., & Gonella, M. (2005). A century of land

subsidence in Ravenna, Italy. Environmental Geology, 47, 831-846.

TCEQ (2009). Indicator bacteria total maximum daily loads for the Brays Bayou watershed. Technical Support Document: Texas Commission on Environmental Quality, 1–59. https://www.tceq.texas.gov/assets/public/waterquality/tmdl/72houmetbact/72-braysbayou-tsd.pdf. Accessed 08 May 2016.

University of Houston & Parsons (2009). Technical Support Document: Indicator Bacteria Total Maximum Daily Loads for the Brays Bayou Watershed, Houston, Texas (1007B_01, 1007C_01, 1007E_01, 1007L_01, 1007B_02). Austin, TX: Texas Commission on Environmental Quality, 2009C.

Verbeiren, B., Van de Voorde, T., Canters, F., Binard, M., Cornet, Y., & Batelaan, O. (2013). Assessing urbanization effects on rainfall-runoff using a remote sensing supported modelling strategy. International Journal of Applied Earth Observation and Geoinformation, 21, 92-102.

Vieux, B. E., & Bedient, P. B. (2004). Assessing urban hydrologic prediction accuracy through event reconstruction. Journal of Hydrology, 299(3-4), 217-236.

Walker, J. (2017, October 27). Subsidence in the Houston-Galveston region: A new tool to learn from the past. Texas Living Waters Project. https://texaslivingwaters.org/houston-subsidence-mapping-tool/

Walker, K., & Shelton, K. (2016). Houston in Flux: Understanding a Decade of Bayou City Development.

Wang, J., Yi, S., Li, M., Wang, L., & Song, C. (2018). Effects of sea level rise, land subsidence, bathymetric change and typhoon tracks on storm flooding in the coastal areas of Shanghai. Science of the total environment, 621, 228-234.

Wang, Y. Q., Wang, Z. F., & Cheng, W. C. (2019). A review on land subsidence caused by groundwater withdrawal in Xi'an, China. Bulletin of Engineering Geology and the Environment,

78, 2851-2863.

Xia, J., Huang, G. H., Chen, Z., & Rong, X. (2001). An integrated planning framework for managing flood-endangered regions in the Yangtze River Basin. Water international, 26(2), 153-161.

Xu, Y. S., Ma, L., Shen, S. L., & Sun, W. J. (2012). Evaluation of land subsidence by considering underground structures that penetrate the aquifers of Shanghai, China. Hydrogeology Journal, 20(8), 1623-1634.

Yager, J., Peri, C., & Rosoff, S. (2017). Population in the US floodplains (Rep.). NYU Furman Center.

Yin, J., Yu, D., Yin, Z., Wang, J., & Xu, S. (2013). Modelling the combined impacts of sea-level rise and land subsidence on storm tides induced flooding of the Huangpu River in Shanghai, China. Climatic change, 119(3-4), 919-932.

Yin, J., Yu, D., & Wilby, R. (2016). Modelling the impact of land subsidence on urban pluvial flooding: A case study of downtown Shanghai, China. Science of the Total Environment, 544, 744-753.

Yu, D., & Lane, S. N. (2011). Interactions between subgrid-scale resolution, feature representation and grid-scale resolution in flood inundation modelling. Hydrological Processes, 25(1), 36-53.

Yu, J., Wang, G., Kearns, T. J., & Yang, L. (2014). Is there deep-seated subsidence in the Houston-Galveston area?. International Journal of Geophysics, 2014.

Zope, P. E., Eldho, T. I., & Jothiprakash, V. (2016). Impacts of land use–land cover change and urbanization on flooding: A case study of Oshiwara River Basin in Mumbai, India. Catena, 145, 142-154.

Appendix
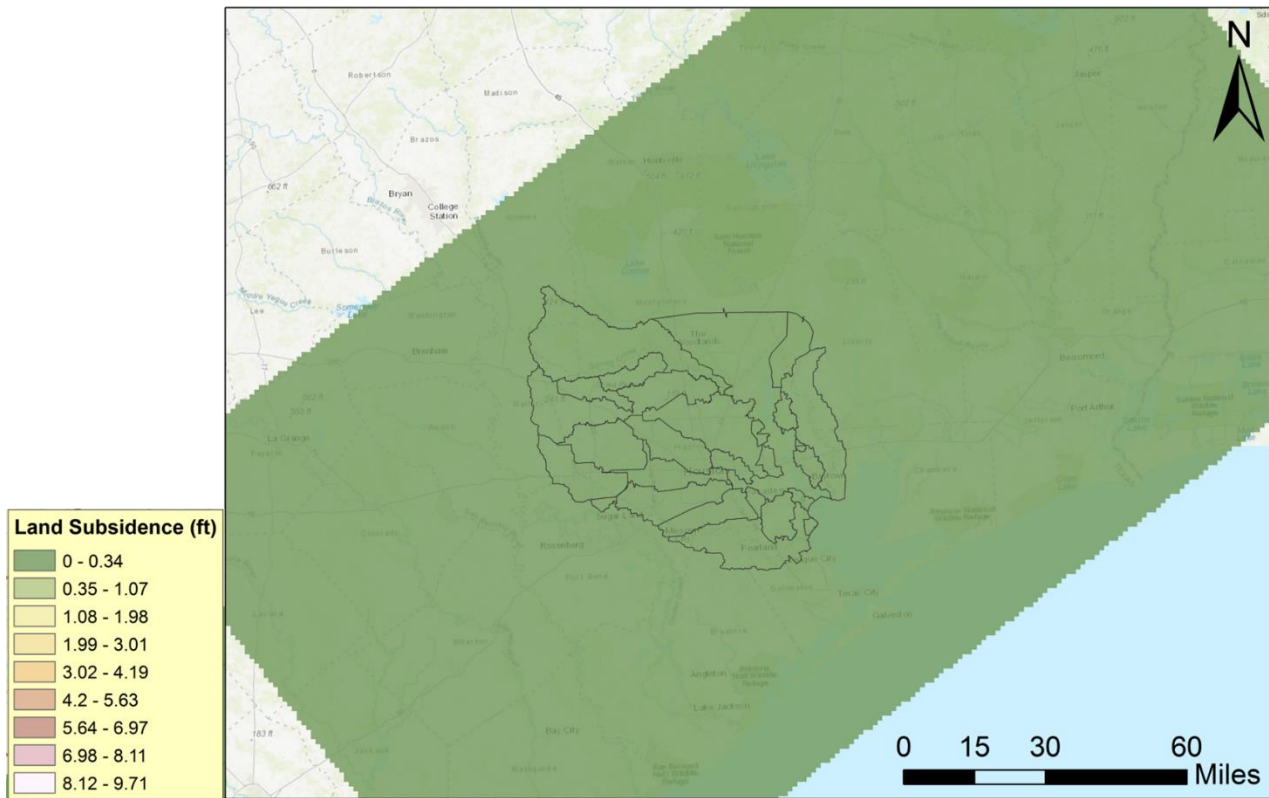
Figure A1: Land subsidence in year 1900.
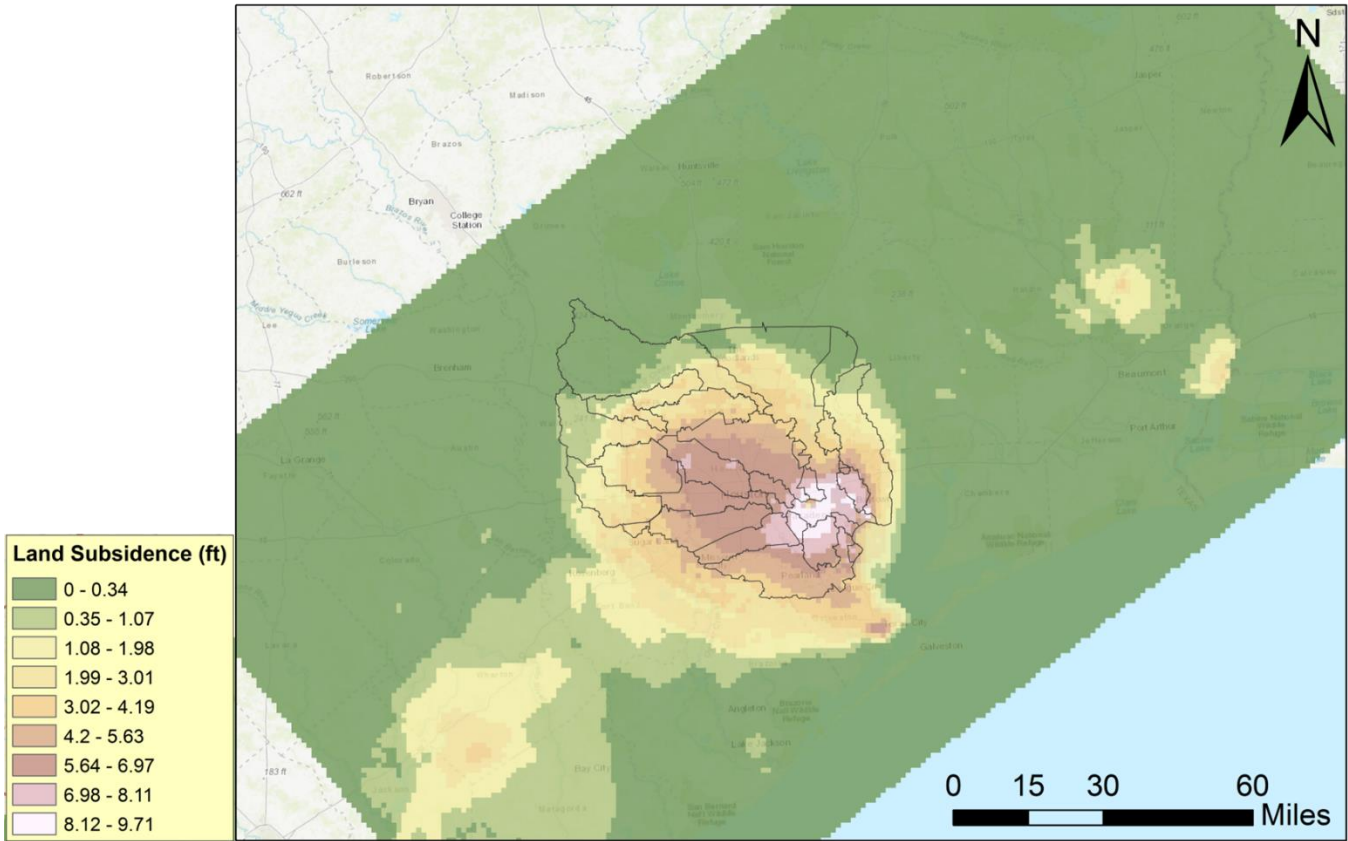
Figure A1: Land subsidence in year 2017.
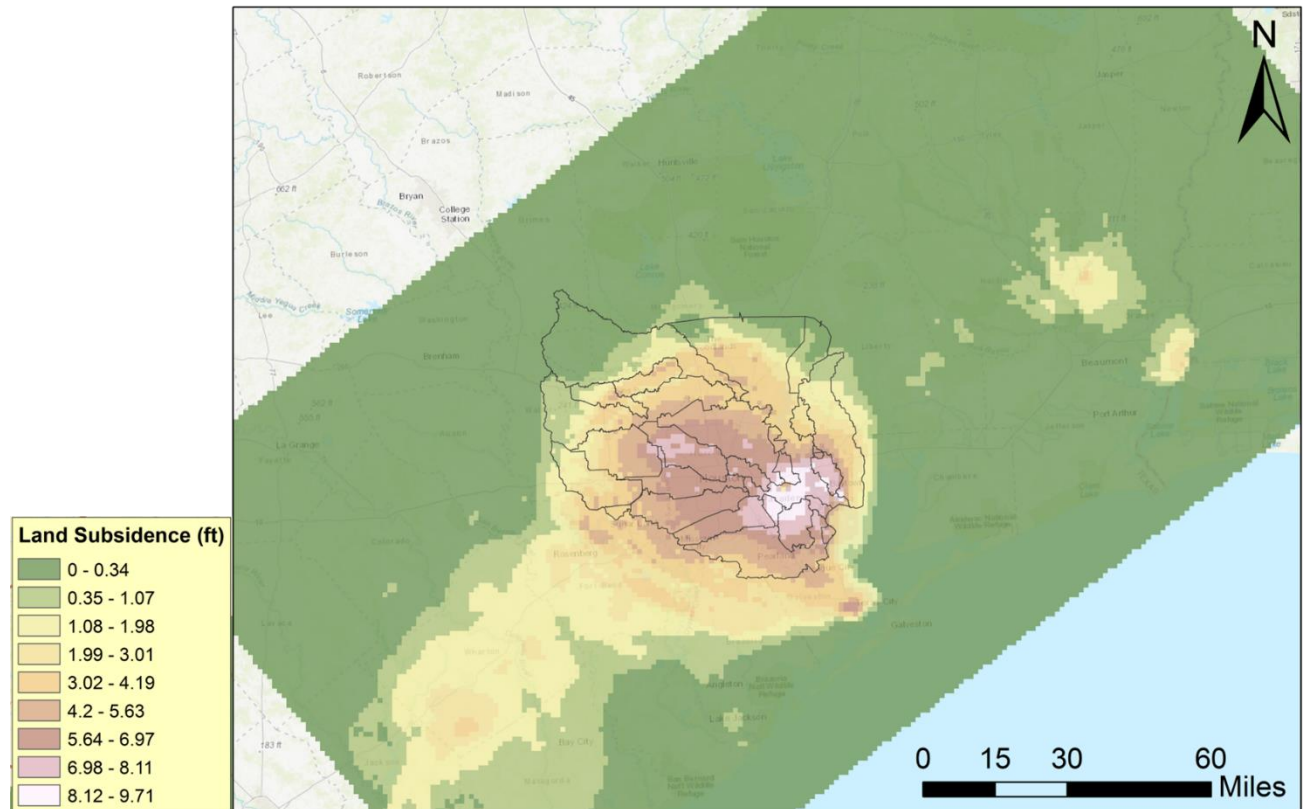
Figure A3: Land subsidence in year 2045.
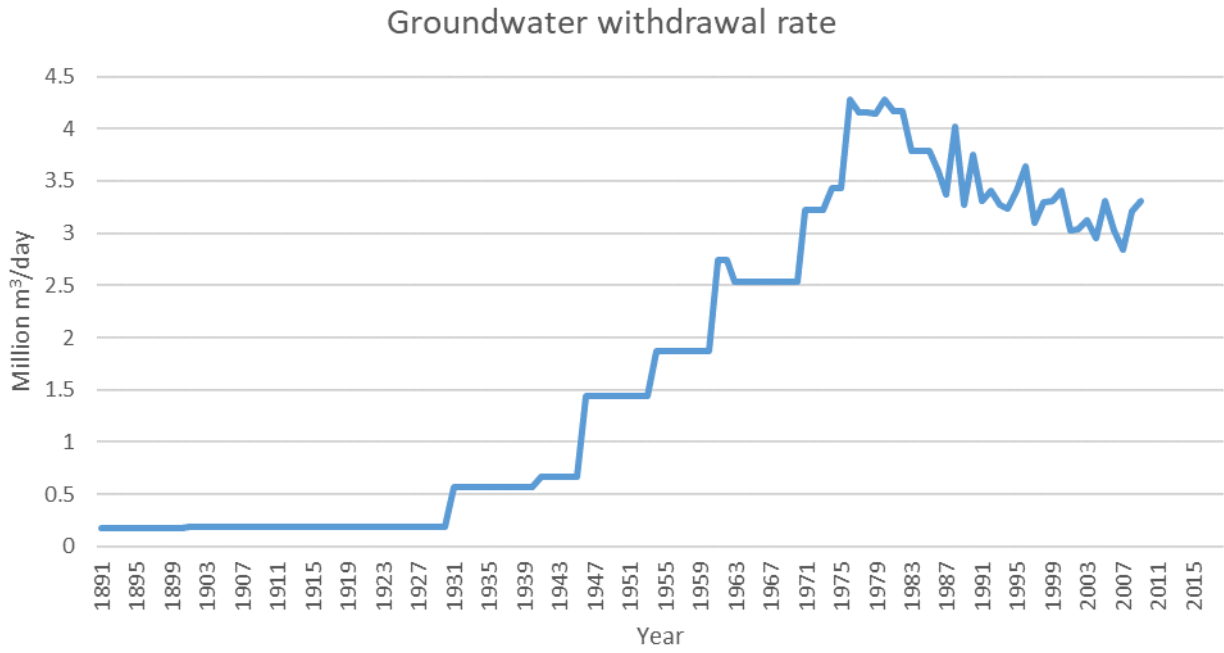
Figure A4: Groundwater withdrawal rate.

Legend

□ BraysBayouBoundary
■ 0 - 1.5
■ 1.51 - 3.5
■ 3.51 - 7.5
■ 7.51 - 15.5
■ 15.51 - 20
■ 20.01 - 30
■ > 30
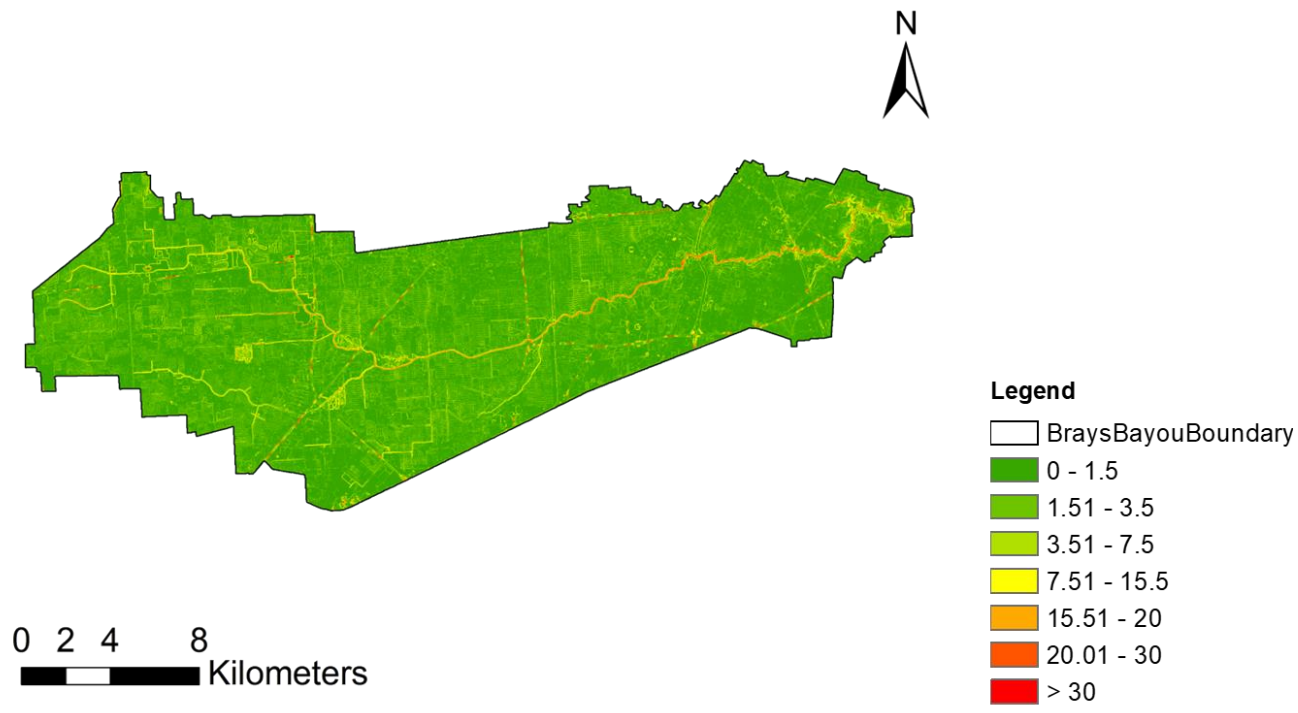
Figure A5: Watershed slope in percentage.
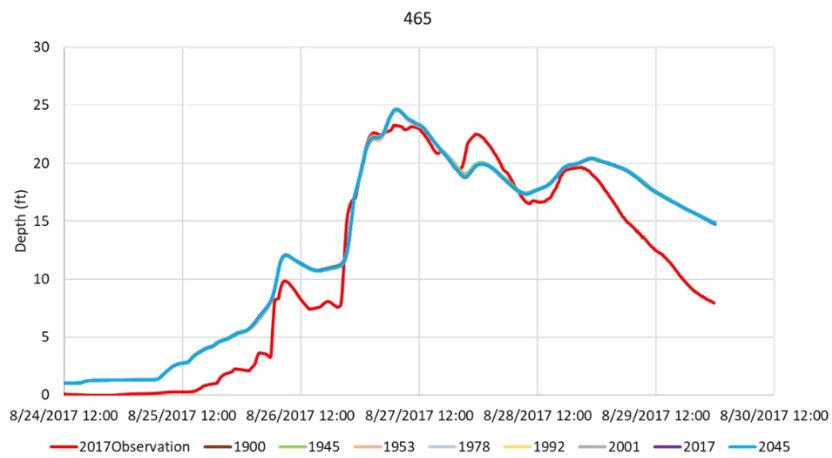
Simulation	Terrain	LC (Manning's N)	Rainfall (Imperviousness)
1	1900	2017	2017
2	1945	2017	2017
3	1953	2017	2017
4	1975	2017	2017
5	1992	2017	2017
6	2001	2017	2017
7	2017	2017	2017
8	2045	2017	2017
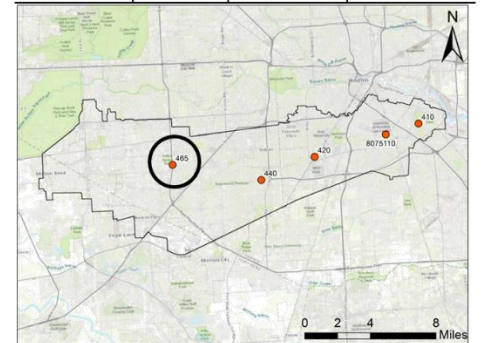
Figure A6: Calibration result at gauge 465 in Scenario 1
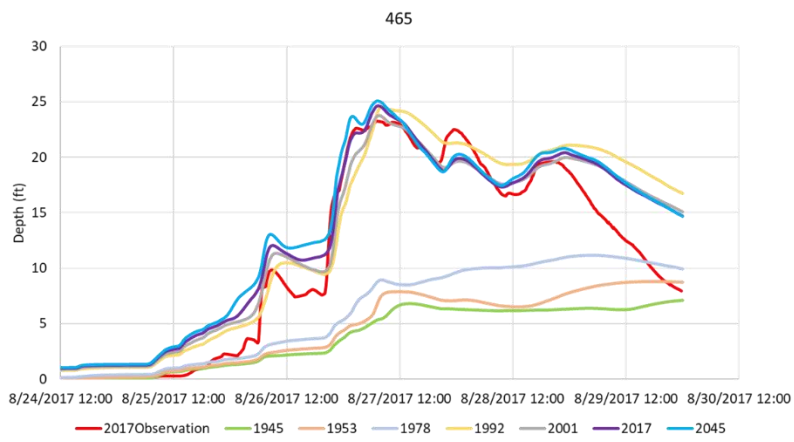
Simulation	Terrain	LC (Manning's N)	Rainfall (Imperviousness)
1	2017	1944	1944
2	2017	1953	1953
3	2017	1978	1978
4	2017	1992	1992
5	2017	2001	2001
6	2017	2045	2045
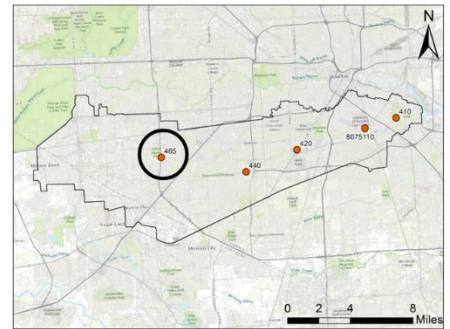
Figure A7: Calibration result at gauge 465 in Scenario 2

a) Scenario 1

	S1-1	S1-2	S1-3	S1-4	S1-5	S1-6	S1-7	S1-8
Median of Maximum Flood Depth (ft)	1.0052	0.9976	0.994	0.9939	1.001	1.0017	1.0045	1.0034

b)
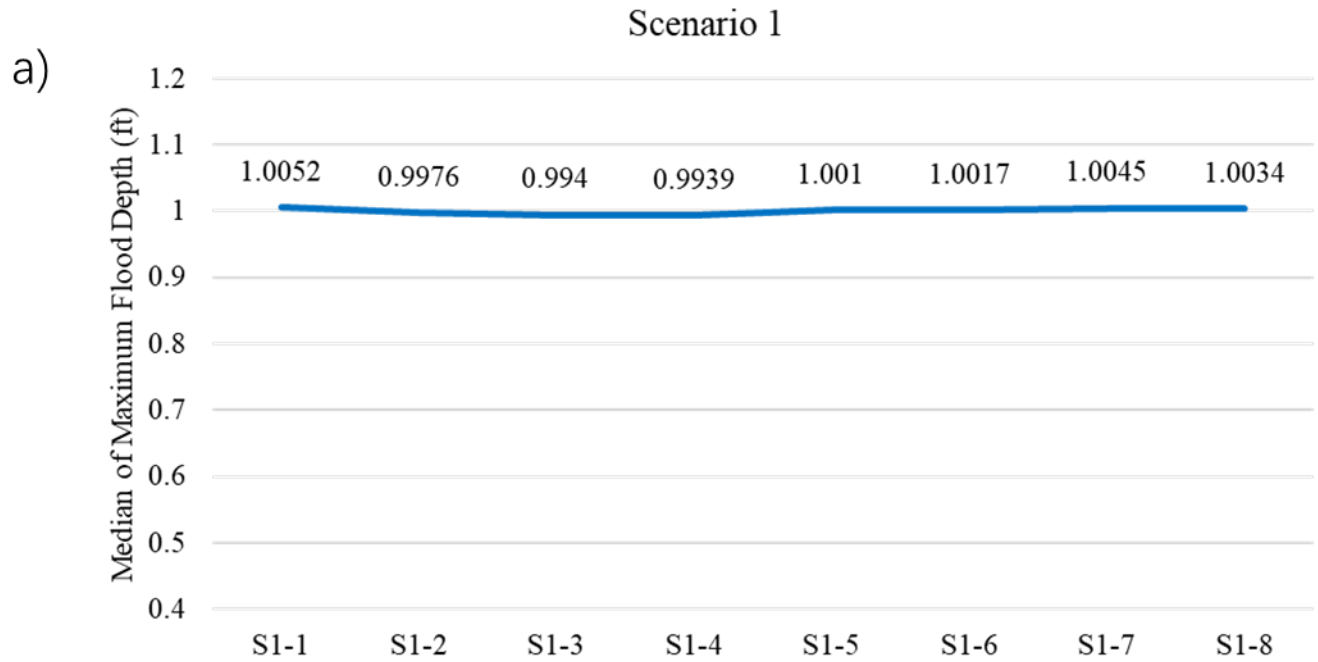
Scenario	Simulation ID	LS	LC (Manning's N)	Rainfall (Imperviousness)
S1	1	1900	2017	2017
	2	1945	2017	2017
	3	1953	2017	2017
	4	1978	2017	2017
	5	1992	2017	2017
	6	2001	2017	2017
	7	2017	2017	2017
	8	2045	2017	2017

Figure A8: Median of Maximum Flood Depth in S1

a)

b)
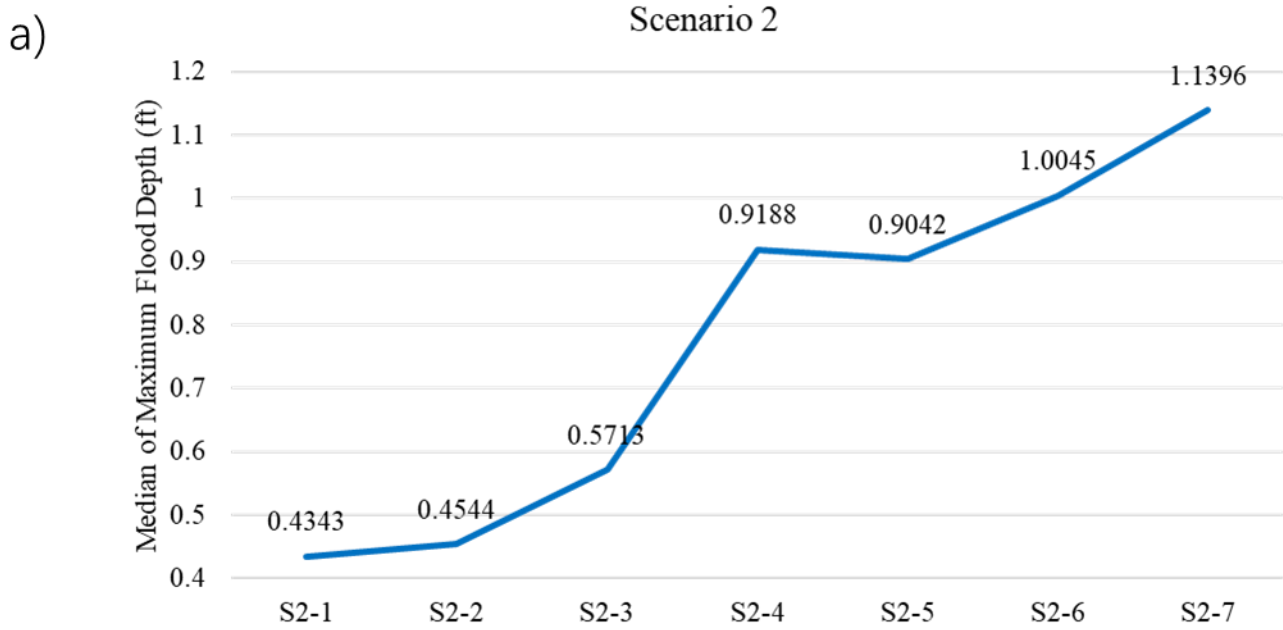
Scenario	Simulation ID	LS	LC (Manning's N)	Rainfall (Impervious ness)
S2	1	2017	1944	1944
	2	2017	1953	1953
	3	2017	1978	1978
	4	2017	1992	1992
	5	2017	2001	2001
	6	2017	2017	2017
	7	2017	2045	2045

Figure A9: Median of Maximum Flood Depth in S2

a)

Scenario 3

b)

Scenario	Simulation ID	LS	LC (Manning's N)	Rainfall (Imperviousness)
	1	1945	1944	1944
	2	1953	1953	1953
	3	1978	1978	1978
S3	4	1992	1992	1992
	5	2001	2001	2001
	6	2017	2017	2017
	7	2045	2045	2045

Figure A10: Median of Maximum Flood Depth in S3
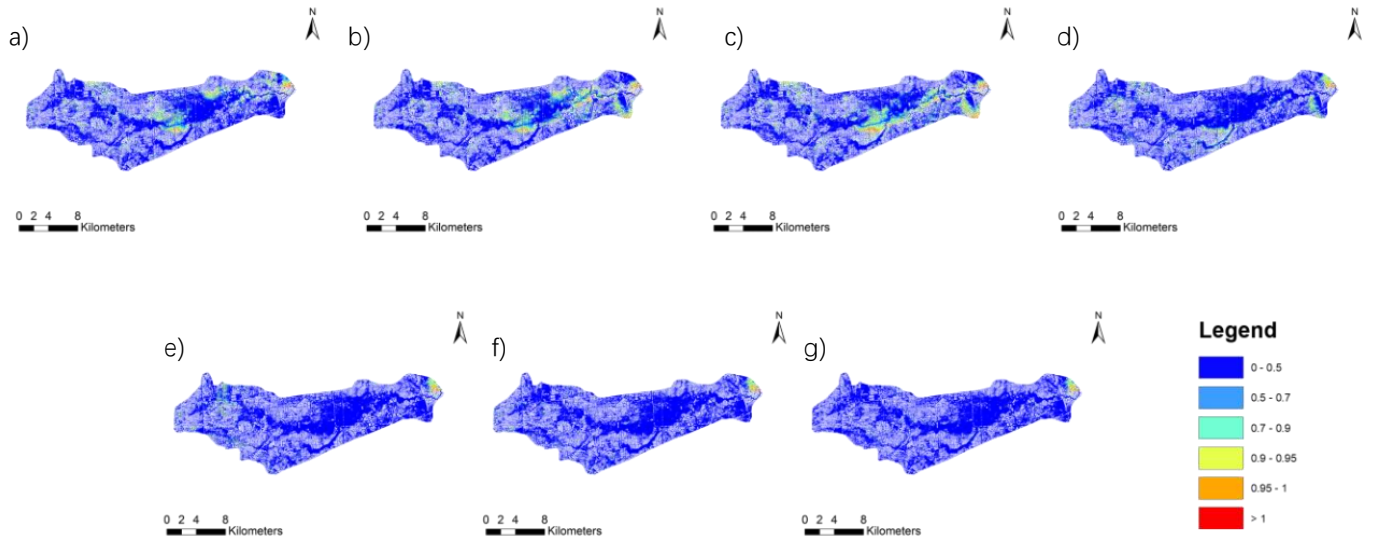
Figure A11: Depth ratio of other years over year 2017 in S1, a) 1900 Terrain, b) 1945 Terrain, c) 1953 Terrain, d) 1978 Terrain, e) 1992 Terrain, f) 2001 Terrain and g) 2045 Terrain

Table a1: Stage Hydrograph at Gauge 410

Reading Date	Elevation (ft)
8/23/17 12:00 PM	1.5
8/23/17 1:00 PM	1.42
8/23/17 2:00 PM	1.32
8/23/17 3:00 PM	1.22
8/23/17 4:00 PM	1.262
8/23/17 5:00 PM	1.304
8/23/17 6:00 PM	1.27
8/23/17 7:00 PM	1.5
8/23/17 8:00 PM	1.653
8/23/17 9:00 PM	1.75
8/23/17 10:00 PM	1.81
8/23/17 11:00 PM	1.527
8/24/17 12:00 AM	1.203
8/24/17 1:00 AM	0.925
8/24/17 2:00 AM	0.647
8/24/17 3:00 AM	0.313
8/24/17 4:00 AM	0.242
8/24/17 5:00 AM	0.17
8/24/17 6:00 AM	0.28
8/24/17 7:00 AM	0.44
8/24/17 8:00 AM	0.793
8/24/17 9:00 AM	1.14
8/24/17 10:00 AM	1.41
8/24/17 11:00 AM	1.63
8/24/17 12:00 PM	1.593
8/24/17 1:00 PM	1.377
8/24/17 2:00 PM	1.18
8/24/17 3:00 PM	1.07
8/24/17 4:00 PM	0.94
8/24/17 5:00 PM	0.903
8/24/17 6:00 PM	0.89
8/24/17 7:00 PM	1
8/24/17 8:00 PM	1.213
8/24/17 9:00 PM	1.533
8/24/17 10:00 PM	1.501
8/24/17 11:00 PM	1.469

8/25/17 12:00 AM	1.437
8/25/17 1:00 AM	1.405
8/25/17 2:00 AM	0.968
8/25/17 3:00 AM	0.809
8/25/17 4:00 AM	0.65
8/25/17 5:00 AM	0.48
8/25/17 6:00 AM	0.6
8/25/17 7:00 AM	0.72
8/25/17 8:00 AM	1.05
8/25/17 9:00 AM	1.268
8/25/17 10:00 AM	1.555
8/25/17 11:00 AM	1.71
8/25/17 12:00 PM	1.63
8/25/17 1:00 PM	1.55
8/25/17 2:00 PM	1.4
8/25/17 3:00 PM	1.21
8/25/17 4:00 PM	1.357
8/25/17 5:00 PM	1.173
8/25/17 6:00 PM	0.88
8/25/17 7:00 PM	1.394
8/25/17 8:00 PM	1.706
8/25/17 9:00 PM	1.942
8/25/17 10:00 PM	2.071
8/25/17 11:00 PM	2.2
8/26/17 12:00 AM	2.103
8/26/17 1:00 AM	2.005
8/26/17 2:00 AM	1.7
8/26/17 3:00 AM	1.6
8/26/17 4:00 AM	1.49
8/26/17 5:00 AM	1.385
8/26/17 6:00 AM	1.583
8/26/17 7:00 AM	1.962
8/26/17 8:00 AM	2.045
8/26/17 9:00 AM	2.689
8/26/17 10:00 AM	3.023
8/26/17 11:00 AM	2.745
8/26/17 12:00 PM	2.85
8/26/17 1:00 PM	2.993

8/26/17 2:00 PM	2.77
8/26/17 3:00 PM	2.82
8/26/17 4:00 PM	2.87
8/26/17 5:00 PM	2.99
8/26/17 6:00 PM	2.763
8/26/17 7:00 PM	3.088
8/26/17 8:00 PM	3.558
8/26/17 9:00 PM	3.88
8/26/17 10:00 PM	4.01
8/26/17 11:00 PM	3.91
8/27/17 12:00 AM	4.215
8/27/17 1:00 AM	4.503
8/27/17 2:00 AM	4.044
8/27/17 3:00 AM	3.75
8/27/17 4:00 AM	3.745
8/27/17 5:00 AM	3.74
8/27/17 6:00 AM	4.339
8/27/17 7:00 AM	6.401
8/27/17 8:00 AM	8.3
8/27/17 9:00 AM	8.317
8/27/17 10:00 AM	8.186
8/27/17 11:00 AM	8.055
8/27/17 12:00 PM	7.603
8/27/17 1:00 PM	6.957
8/27/17 2:00 PM	6.151
8/27/17 3:00 PM	5.335
8/27/17 4:00 PM	4.807
8/27/17 5:00 PM	4.533
8/27/17 6:00 PM	4.29
8/27/17 7:00 PM	4.502
8/27/17 8:00 PM	4.714
8/27/17 9:00 PM	4.925
8/27/17 10:00 PM	11.298
8/27/17 11:00 PM	16.784
8/28/17 12:00 AM	18.34
8/28/17 1:00 AM	19.208
8/28/17 2:00 AM	19.25
8/28/17 3:00 AM	19.097

8/28/17 4:00 AM	19.611
8/28/17 5:00 AM	20.226
8/28/17 6:00 AM	20.43
8/28/17 7:00 AM	20.554
8/28/17 8:00 AM	20.514
8/28/17 9:00 AM	20.492
8/28/17 10:00 AM	20.47
8/28/17 11:00 AM	20.333
8/28/17 12:00 PM	20.321
8/28/17 1:00 PM	20.31
8/28/17 2:00 PM	20.267
8/28/17 3:00 PM	20.205
8/28/17 4:00 PM	20.051
8/28/17 5:00 PM	19.898
8/28/17 6:00 PM	19.432
8/28/17 7:00 PM	19.113
8/28/17 8:00 PM	18.667
8/28/17 9:00 PM	18.655
8/28/17 10:00 PM	19.612
8/28/17 11:00 PM	20.37
8/29/17 12:00 AM	20.41
8/29/17 1:00 AM	20.26
8/29/17 2:00 AM	19.99
8/29/17 3:00 AM	19.488
8/29/17 4:00 AM	18.933
8/29/17 5:00 AM	18.578
8/29/17 6:00 AM	18.286
8/29/17 7:00 AM	18.055
8/29/17 8:00 AM	17.756
8/29/17 9:00 AM	17.36
8/29/17 10:00 AM	17.5
8/29/17 11:00 AM	17.387
8/29/17 12:00 PM	17.273
8/29/17 1:00 PM	17.035
8/29/17 2:00 PM	17.303
8/29/17 3:00 PM	17.782
8/29/17 4:00 PM	18.057
8/29/17 5:00 PM	18.465

8/29/17 6:00 PM	18.39
8/29/17 7:00 PM	18.502
8/29/17 8:00 PM	18.613
8/29/17 9:00 PM	19.108
8/29/17 10:00 PM	19.085
8/29/17 11:00 PM	19.063
8/30/17 12:00 AM	18.643
8/30/17 1:00 AM	18.6
8/30/17 2:00 AM	18.48
8/30/17 3:00 AM	18.183
8/30/17 4:00 AM	17.817
8/30/17 5:00 AM	17.43
8/30/17 6:00 AM	16.817
8/30/17 7:00 AM	16.218
8/30/17 8:00 AM	15.522
8/30/17 9:00 AM	14.96
8/30/17 10:00 AM	14.4
8/30/17 11:00 AM	13.848
8/30/17 12:00 PM	13.313
8/30/17 1:00 PM	12.947
8/30/17 2:00 PM	12.585
8/30/17 3:00 PM	12.177
8/30/17 4:00 PM	11.91
8/30/17 5:00 PM	11.613
8/30/17 6:00 PM	11.277
8/30/17 7:00 PM	11.015
8/30/17 8:00 PM	10.73
8/30/17 9:00 PM	10.475
8/30/17 10:00 PM	10.29
8/30/17 11:00 PM	10.075
8/31/17 12:00 AM	9.91

Table a2: Fit statistics during time periods

	Ao	Ar		As		F
1900	-			-	-	-
1930	1993417645			1853723	1995322849	0.99811313
1945	1981954126			1850241	1991574871	0.988554307
1960	1976116881			1845860	1986859220	0.985091733
1970	1973740219	1853684	1995280870	1845438	1986404985	0.982964968
1980	1968281862			1846919	1987999114	0.97681573
1990	1972150396			1851508	1992938653	0.978215662
2000	1974393586			1852431	1993932158	0.979935742
2010	1975115841			1852859	1994392851	0.980421491
2017	1972683207			1853182	1994740524	0.977864405

Table a3: RMSD of Flood Depth

Year	Depth RMSD (ft)	Depth RMSD (m)
1930	0.015	0.004572
1945	0.0669	0.02039112
1960	0.077	0.0234696
1970	0.085	0.025908
1980	0.125	0.0381
1990	0.118	0.0359664
2000	0.1064	0.03243072
2010	0.1063	0.03240024
2017	0.108	0.0329184